Journal of Catalysis 450 (2025) 116231

Contents lists available at ScienceDirect

Journal of Catalysis

journal homepage: www.elsevier.com/locate/jcat

Research article

Carbon dioxide hydrogenation to formate catalyzed by highly active Ru-tris (pyrazolyl)methane complexes

Sylwia Kostera [a,1], Alberto Gobbo [b,1], Massimo Guelfi [b], Stefano Zacchini [c], Gabriele Manca [a], Fabio Marchetti [b,*], Luca Gonsalvi [a,*]

[a] Consiglio Nazionale delle Ricerche (CNR), Istituto di Chimica dei Composti Organometallici (ICCOM), Via Madonna del Piano 10, 50019 Sesto Fiorentino, Florence, Italy
[b] University of Pisa, Department of Chemistry and Industrial Chemistry, Via G. Moruzzi 13, 56124 Pisa, Italy
[c] University of Bologna, Department of Industrial Chemistry "Toso Montanari", Via P. Gobetti 85, 40129 Bologna, Italy

ARTICLE INFO

Keywords:
CO_2 hydrogenation
Ruthenium complexes
Tris(pyrazolyl)methane
Homogeneous catalysis
Mechanistic studies

ABSTRACT

In the quest for novel, active ruthenium(II) complexes for homogeneous catalytic CO_2 hydrogenation to formate, a small library of cationic Ru(κ^3-tpm) complexes [tpm = tris(pyrazolyl)methane] bearing different ancillary ligands were tested under various reaction conditions, with and without the addition of a Lewis acid co-catalyst. Under optimized conditions (80 bar, 120 °C) and in the presence of LiOTf, TONs > 54000 were obtained in single batch runs with the complex [RuCl(κ^3-tpm)(PPh_3)(CH_3CN)]Cl (**1**). Mechanistic studies using NMR spectroscopy and DFT calculations were also carried out to elucidate key steps and the energies associated with the reaction pathway, which allowed for the proposal of a catalytic mechanism.

1. Introduction

CO_2 is a component of the Earth's atmosphere that is essential for photosynthesis in plants. Its steady increase over the past century, from about 280 parts per million (ppm) to over 415 ppm today, is primarily due to human activities, particularly the combustion of fossil fuels such as coal, oil, and gas. This increase is contributing to global warming, climate change and ocean acidification [1]. While CO_2 capture and storage (CCS) is an option under study to help in environmental remediation, it has significant drawbacks, such as high costs and low acceptance levels by the general public. In this view, and in combination with the need of sustainable production, researchers worldwide are advocating for the reuse of CO_2 as a cheap, safe, and abundant feedstock for producing chemicals on both laboratory and larger scales (CCU technologies) [2]. The reduction of CO_2 to C1 derivatives such as formic acid, formaldehyde, methanol and methane is a viable pathway for CO_2 utilization [3]. Among these, methanol (CH_3OH) and formic acid (HCOOH) are considered as potential future fuels and liquid organic hydrogen carriers (LOHCs), respectively. LOHCs represent a form of "stored" hydrogen that can be released on demand through dehydrogenation reactions in the presence of suitable catalysts, providing a sustainable, carbon–neutral cycle for hydrogen storage and delivery [4].

The global demand for formic acid is increasing, particularly in the Asian market, due to its various applications [5]. Currently, industrial production of HCOOH occurs through the hydrolysis of methyl formate, which is typically derived from fossil-based feedstock. A sustainable alternative synthesis using renewable, non-fossil-based feedstocks, such as the reaction between CO_2 and H_2, is thus of great interest. In the gas phase, CO_2 hydrogenation is endergonic owing to entropic factors, but it becomes exergonic in the presence of strong bases and/or polar solvents [6]. Additionally, CO_2 is chemically inert, and activating it requires the use of efficient catalysts. Precious and non-precious metals heterogeneous and homogeneous catalysts for CO_2 hydrogenation have been developed and studied by numerous research groups worldwide. Homogeneous catalysts, based on tailored organometallic and/or coordination complexes, offer simpler synthetic tunability compared to their heterogeneous counterparts, providing higher process selectivities under milder pressures and temperatures. Over the past 40 years,

Abbreviations: CCS, CO_2 capture and storage; CCU, Carbon Capture and Utilisation; LOHC, Liquid organic hydrogen carriers; tpm, tris(pyrazolyl)methane; Tp, tris(pyrazolyl)borate; TON, turnover number; TOF, Turnover Frequency; THF, tetrahydrofuran.

* Corresponding authors.
E-mail addresses: fabio.marchetti@unipi.it (F. Marchetti), l.gonsalvi@iccom.cnr.it (L. Gonsalvi).

[1] These authors equally contributed to this work.

https://doi.org/10.1016/j.jcat.2025.116231
Received 26 March 2025; Received in revised form 15 May 2025; Accepted 16 May 2025
Available online 21 May 2025

research in this area has yielded remarkable advancements in catalyst design and process optimization, significantly improving efficiency and expanding our knowledge base [4,6,7].

Most transition metals have been tested over the years for homogeneous CO_2 hydrogenation, in combination with various classes of stabilizing ligands, including mono-, bi-, and tridentate phosphines or aminophosphines, pincer-type ligands, η^6-arenes, cyclopentadienyls and bipyridines, and others. Among precious platinum group metals, Ru and Ir have shown the highest performances [7]. In recent years, there has been a growing interest in the study of CO_2 hydrogenation to formates using earth-abundant metal complexes, principally Fe [8], Co [9], Mn [10] and Ni [11], as cheaper alternatives to noble metals, reaching very high productivities. In spite of this, precious metals are still the most widely applied for this class of reactions. Selected examples of literature data for some of the most highly active homogeneous catalysts for CO_2 hydrogenation to formates are summarized in Table 1.

In the case of ruthenium-catalyzed CO_2 hydrogenation to formate, the state-of-the-art is currently held by Pidko and co-workers with the pincer-type complex [RuH(Cl)(CO)(PNP-^{t}Bu)] as catalyst [PNP-^{t}Bu = 2,6-Bis(di-*tert*-butylphosphinomethyl)pyridine], achieving outstanding TON = 200,000 and TOF = 1,100,000 h^{-1} in the presence of 1,5-diazabicyclo(5.4.0)undec-7-ene (DBU) as a base, *N,N*-dimethylformamide (DMF) as solvent, 60 bar H_2/CO_2 (3:1), and 120 °C [12]. Pincer-type molecules are among the most widely used ligands for their unique donor properties, such as their exclusively meridional coordination to the metal and the easy tunability of electronic and steric properties by proper choice of functional group substituents and donor atoms, particularly phosphorus and nitrogen (PNP ligands). Drawbacks include, in some cases, the use of expensive chemical synthons, endangered elements such as phosphorus, multi-step synthetic pathways, and lengthy product purifications. On the other hand, polydentate phosphine ligands are challenging to functionalize and are prone to oxidation, whereas η^6-arenes are often observed to be labile under forcing reaction conditions, leading to catalyst decomposition.

A well-known class of potentially tridentate *N,N,N*-capping ligands is represented by tris(pyrazolyl)-based molecules, generally referred to as

Table 1
Selected examples of homogeneous catalysts for CO_2 hydrogenation to formates.[a]

Catalyst	pH_2/pCO_2 (bar)	Temp. [°C]	Solvent	Base	Additive	Highest TON	Highest TOF (h^{-1})	Ref.
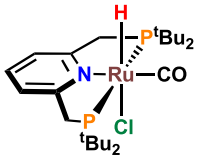	30/10	120	DMF	DBU	–	200,000	1,100,000	[12]
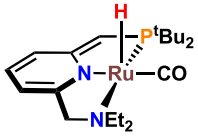	30/10	200	diglyme	K_2CO_3	–	23,000	2200	[13]
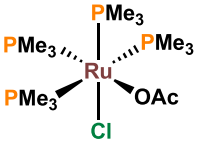	70/120	50	$scCO_2$/C_6F_5OH	NEt_3	–	32,000	95,000	[14]
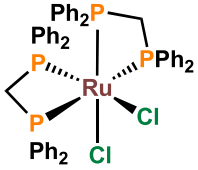	60/30	70	H_2O/MIBC	NEt_3	–	14,540	35,000	[3b]
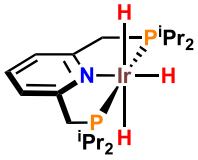	30/30	120	THF	KOH	–	3,500,000	150,000	[15]
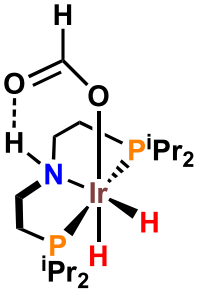	28/28	185	H_2O	KOH	–	348,000	14,500	[16]

(*continued on next page*)

Table 1 (*continued*)

Catalyst	pH_2/pCO_2 (bar)	Temp. [°C]	Solvent	Base	Additive	Highest TON	Highest TOF (h^{-1})	Ref.
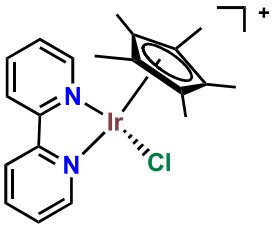	30/30	120	H_2O	KOH	–	190,000	42,000	[17]
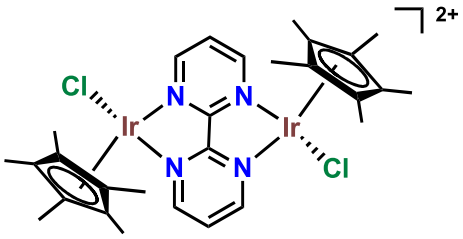	25/25	80	H_2O	$KHCO_3$	–	79,000	53,800	[18]
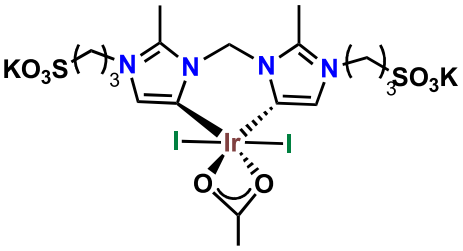	30/30	200	H_2O	KOH	–	190,000	2500	[19]
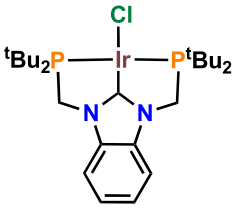	25/25	120	THF	N $(CH_2CH_2OH)_3$	–	230,000	5000	[20]
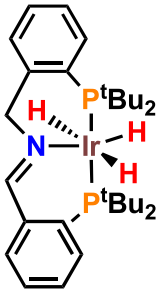	40/20	140	THF/H_2O	KOH	–	450,000	22,500	[21]
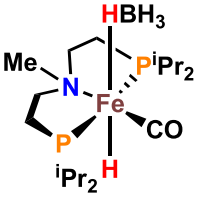	35/35	80	THF	DBU	LiOTf	58,990	2458	[8b]
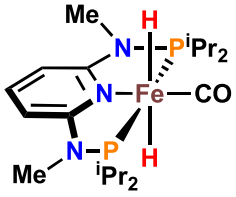	40/40	80	EtOH	DBU	–	10,275	489	[8a]

(*continued on next page*)

Table 1 (*continued*)

Catalyst	pH_2/pCO_2 (bar)	Temp. [°C]	Solvent	Base	Additive	Highest TON	Highest TOF (h^{-1})	Ref.
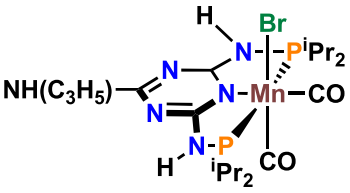	60/20	115	THF/H_2O	Lysine	–	230,000	19,167	[10b]
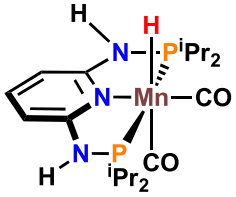	40/40	100	THF/H_2O	DBU	LiOTf	31,600	1317	[10g]
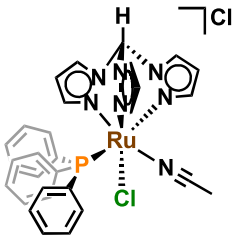	40/40	120	^{i}PrOH	DBU	LiOTf	54,169	5940	This work

[a] Pressure, temperature, solvent, base, additive, TON and TOF data and values refer to the reported optimized conditions, applied in single batch experiments. $scCO_2$ = supercritical CO_2. MIBC = methyl isobutyl carbinol.

scorpionate ligands [22]. These all-N ligands promote facial coordination to metals and, depending on the bridgehead atom, can be either neutral (C atom) or anionic (B atom). These two sub-classes are termed tris(pyrazolyl)methane (tpm) and tris(pyrazolyl)borate (Tp), respectively. These ligands behave as σ-donors, forming strong tridentate bonds with the metal through three nitrogen atoms, contrasting with traditional metal-arene interactions that involve π-back-donation [23,24]. Hemilabile κ^3- to κ^2-coordination behavior has been observed for Ru(tpm) complexes in some cases and has recently been exploited by some of us in the catalytic transfer hydrogenation of ketones [24d].

To the best of our knowledge, only a few examples of CO_2 homogeneous hydrogenation protocols in the presence of metal scorpionate ligands have been reported so far. In 2001, Lin, Lau and coworkers showed that hydrogenation of CO_2 to formic acid with complex [TpRuH(PPh_3)(CH_3CN)], NEt_3, THF/H_2O (3:1); 50 bar CO_2/H_2 (1:1), 100 °C reached TON = 760 after 16 h, and that the addition of water was beneficial to increase catalytic efficiency [25]. In 2004, Lau and coworkers expanded on the previous study, testing the same complex as catalyst under different reaction conditions and solvents. It was observed that the activity of [TpRuH(PPh_3)(CH_3CN)] is higher in CF_3CH_2OH than in methanol and other non-acidic alcohols (max TON = 1815), likely due to the enhanced electrophilicity of the carbon atom of CO_2 in this solvent. Mechanistic studies suggested that HCOOH is formed upon hydride and proton transfer from the transient alcohol hydride intermediate [TpRuH(PPh_3)(ROH)] to the incoming CO_2 [26]. Finally, Martins and coworkers demonstrated in 2017 the successful use of the Fe(II)-tpm complex [$FeCl_2$(κ^3-tpm)] in the one-pot CO_2 hydrogenation to CH_3OH (44 % yield, TONs up to 2300) in the presence of pentaethylenehexamine (PEHA) as a base, 75 bar CO_2/H_2 (1:3), 80 °C, 48 h [27].

Inspired by these results, we jointly investigated the applicability of a library of cationic Ru(tpm) complexes (Fig. 1) as catalysts for CO_2 hydrogenation to formate. The main catalytic results are hereby described together with mechanistic details obtained through a combination of experimental techniques (NMR) and Density Functional Theory (DFT) calculations.

2. Results and discussion

2.1. Synthesis of novel Ru tris(pyrazolyl)methane complexes

Complex [RuCl(κ^3-tpm)(PPh_3)$_2$]Cl (**4**) was synthesized from ruthenium trichloride and tpm [28a], whereas complex **7** was obtained from a suspension of [$RuCl_3$(κ^3-tpm)]•1.5 H_2O and Zn dust in CH_3CN [29], both according to previously described methods. Complex **4** served as a precursor for the known mono-cationic derivatives **1**–**3** and **5** (Fig. 1), upon the substitution of one PPh_3 with other chosen ligands, in ethanol or isopropanol as solvents at reflux temperature [24d],[28]. Similarly, the unprecedented mono-cationic complex **6** was obtained in 98 % yield. Additionally, the new family of bis-cationic complexes **8**–**10** was synthesized from **4** upon thermal reaction with the appropriate bidentate ligand in ethanol solutions (**8**–**10**). The addition of 2 equivalents of silver nitrate was required to ensure the removal of the chloride ligand and the incorporation of two nitrates as counteranions. Complexes **8**–**10** were isolated in high yields (82–96 %) after work-up; they are well-soluble in alcohols (including methanol and ethanol), fairly-soluble in chlorinated solvents and water, and insoluble in hexane, toluene, diethyl ether and THF. The novel complexes **6, 8**–**10** were characterized by elemental analysis and IR spectroscopy in the solid state, and by multinuclear NMR spectroscopy in various solvents (see Experimental Section). The isocyanide ligand in **6** manifests itself with a strong infrared absorption at 2133 cm^{-1} ($\tilde{\upsilon}$ = 2125 cm^{-1} for uncoordinated 4-methoxyphenylisocyanide in CH_2Cl_2), indicating weak back-donation from the ruthenium(II) center [30]. The IR spectra of **8**–**10** (Figs. S2–S4 in the Supporting Information) display an intense, broad band at 1315–1377 cm^{-1} accounting for the nitrate anions. The NMR spectra of **6, 8**–**10** (Figs. S5–S16) showed the presence of single species in solution, and their main features are substantially in line with those reported for **1**–**5**. ^{1}H and ^{31}P NMR experiments revealed the stability of **8**–**10** in D_2O, with spectra appearing substantially unchanged over 72 h.

Interestingly, the –NH_2 groups in **8** undergo progressive deuterium-exchange in D_2O, as suggested by the disappearance of the ^1H signal at 4.23 ppm after 72 h (Fig. S17), presumably favored by the double cationic charge of the complex.

The structures of **8**–**10** were confirmed by single-crystal X-ray diffraction analyses (Fig. 2 and Table S1 in the Supporting Information). The molecular structure of the cation of **10** was previously reported in a private communication as its [Ru(κ^3-tpm)(PPh_3)(phen)][BF_4]$_2$·0.5acetone salt, together with the related [Ru(κ^3-tpm)(PPh_3)(bipy)][BF_4]$_2$·0.5acetone complex [31]. Cations **8**–**10** display distorted octahedral geometry, as shown by the analysis of δ values (Table S1 and Fig. S71) [32], with the N-Ru-N angles involving the tridentate tris(pyrazolyl)methane ligand smaller than 90°, similar to related complexes [24d],[28],[33]. The bonding parameters of **8**–**10** are very similar to those reported for the two bis-cationic [Ru(κ^3-tpm)(PPh_3)(N-N)]$^{2+}$ (N-N=bidentate N-ligand) complexes previously reported [31]. Replacement of Cl^- with a neutral N-ligand does not seem to significantly affect the structure. The Ru1-N1 bond [2.156(5), 2.123(6) and 2.1137(18) Å for **8**, **9** and **10**, respectively] *trans* to PPh_3 is longer than Ru1-N3 [2.079(5), 2.091(7) and 2.0825(18) Å] and Ru1-N5 [2.085(5), 2.082(7) and 2.0750(18) Å] *trans* to N-ligands. The Ru1-N7 [2.023(4), 2.120(5), 2.056(7) and 2.0679(18) Å] and Ru1-N8 [2.022(4), 2.115(5), 2.109(6) and 2.0588(18) Å] bonding distances reflect the hybridization of nitrogen, being Ru-N(sp) < Ru-N(sp^2) < Ru-N(sp^3). Hydrogen bonds are present within the crystal structures of **8·H_2O** and **9·solv** (see Tables S2–S3 and Fig. S72), involving the NH_2 groups of the cations, the nitrate anions and H_2O molecules.

2.2. Catalytic tests

CO_2 hydrogenation tests (Scheme 1) were initially carried out in the presence of [RuCl(κ^3-tpm)(PPh_3)(CH_3CN)]Cl (**1**) under the conditions previously applied by Lau and coworkers with [TpRuH(PPh_3)(CH_3CN)], *i.e.* using NEt_3 as base (1103 equiv.), under H_2/CO_2 (1:1) at a total pressure of 60 bar, at 100 °C for 24 h, instead of 16 h as reported for the Tp analogue [26]. In solvents such as THF, THF/H_2O or toluene, no activity was observed (Table 2, entries 1–3). Using methanol as a solvent, only traces of product were detected (Table 2, entry 4).

Reaction conditions were then changed, adopting parameters recently applied by some of us for CO_2 hydrogenation in the presence of [Mn(PNP)($CO)_3$], *i.e.* using DBU as base (1000 equiv. to **1**), H_2/CO_2 (1:1) 60 bar total pressure, 100 °C instead 80 °C for 24 h [34]. In the first screening of reaction parameters, the choice of best solvent was assessed. Using dry MeOH as solvent and a **1**/DBU ratio of 1:1000, formate was obtained in 17 % yield (Table 2, entry 5) with respect to DBU, with a corresponding TON = 167. In the case of **4**, the use of methanol also led to low TON = 183 (Table 2, entry 10). By changing the solvent to ^{i}PrOH, formate was obtained with high yield ≥99 % (entry 6) in the case of complex **1** and 90 % in the presence of **4** (entry 11). The use of KO^{t}Bu as a base did not afford formate with satisfactory yields (17 %, entry 7). Based on these results, dry ^{i}PrOH was chosen as solvent for the rest of the study. Next, the screening of other complexes bearing the six-electron donor tpm ligand was tested. Very good yields (93 %) were obtained after 24 h with **2** and **3**. Complexes **5**–**10** showed lower activity compared to **4**, as summarized in Table 2. Negligible activities were observed using **9**/DBU and **10**/DBU ratio to 1:1000, 60 bar, 100 °C, 24 h, with only 9 % yield, TON = 89 and 1 % yield, TON = 11, respectively (entries 16 and 17), likely due to the absence of hemilability of the aminopyridine and phenanthroline ancillary ligands. This indicates that the generation of a vacant coordination site is crucial for substrates activation. Selected results are summarized in Table 2 and visualized as bar graph in Fig. 3.

Fig. 4 shows the trend of activities of complexes increasing from **1** to **10** under the conditions described above. It can be observed that although the synthetic precursor **4** also exhibited good catalytic activity, the highest activity was demonstrated by complex **1,** containing, in addition to triphenylphosphine and κ^3-tpm, chlorine and acetonitrile as co-ligands. This can be attributed to an optimal combination of suitable monodentate donor ligands that, under reaction conditions, are labile enough to undergo substitution by solvents and substrates, which are key steps in the catalytic cycle (*vide infra*).

Next, the effects of catalyst/DBU ratio and temperature were tested, both in the absence of and in the presence of a Lewis acid (LA), at different catalyst/LA ratios (Table 3), under the same pressure and time applied above (60 bar total pressure, 24 h). The effect of adding a Lewis acid (LA) as a co-catalyst was examined in the presence of selected Ru complexes, specifically **1**, **4,** and **6**. With base metals complexes, it was previously demonstrated that LA additives can favor accessible transition states in CO_2 hydrogenation reaction pathways [10g],[35]. More recently, this effect was studied by DFT calculations for other classes of transition metal complexes, including precious metal based ones [36]. To the best of our knowledge, the present study is the first experimental report describing the testing of a lithium salt LA as co-catalyst in CO_2 hydrogenation in the presence of ruthenium complexes. Consistent with the method previously applied with iron [8b] and manganese catalysts [10g], LiOTf ($^-$OTf = $CF_3SO_3^-$) was chosen as LA to promote CO_2 hydrogenation to formate, using 60 bar of H_2/CO_2 = 1:1 gas mixture and testing different catalyst/DBU ratios [34].

Initially, catalyst concentration effects were tested in the absence of LiOTf. Using a **4**/DBU ratio of 1:1000, formate was obtained in 91 % yield, with TON = 910 (Table 3, entry 1). Next, the amount of catalyst was decreased to **4**/DBU ratios of 1:2000, 1:5000, and 1:10,000 (entries 2, 4 and 7, respectively), running the tests at 60 bar, 100 °C, 24 h. At an optimal 1:5000 ratio, TON increased to 3427, albeit with a decreased yield = 68 %. Lower **4**/DBU ratio led to modest results (TON = 3362, yield = 33 %, entry 7).

In the case of complex **6**, with a **6**/DBU ratio of 1:1000 and without Li, formate was obtained in 63 % yield with TON = 628 (entry 8). In another test run for 48 h (entry 9), higher yield (74 %) and TON = 741 were obtained under the same conditions. Upon the addition of LiOTf (1 mmol, **6**/LiOTf = 1:100), formate was obtained in 81 % yield (TON = 816, entry 10) after 24 h. Also in the case of **7**, addition of LiOTf gave formate yield (94 %) and TON enhancement (entry 11, Table 3) compared to the values obtained in its absence (53 % yield, TON = 530, entry 14, Table 2) in catalytic tests run at 100 °C, 24 h.

Next, **1**/DBU ratios of 1:1000 and 1:2000 were tested, and formate was obtained in ≥99 % yield in both cases, with TON = 1004 and 2008, respectively (entries 12 and 13, respectively). The effect of catalyst concentration in the presence of LiOTf was then tested with **1**. A preliminary assessment of the lower limit of catalyst amount needed to achieve the significant yield was carried out initially without LA, and the amount of catalyst was decreased to **1**/DBU ratios of 1:5000 and 1:10,000 under 60 bar H_2/CO_2 (1:1), 100 °C, 24 h (entries 14 and 15, respectively). At a **1**/DBU = 1:5000 ratio, TON increased to 4245 with a slight yield decrease to 84 %, whereas **1**/DBU = 1:10,000 ratio gave TON = 3436 (entry 15). In the presence of added LiOTf (1.0 mmol, **1**/LiOTf = 1:1000, **1**/DBU = 1:10,000), formate was obtained in 58 % yield (TON = 5857, entry 16) after 24 h. The **1**/LiOTf ratio was then varied in three different runs (entries 16–18, respectively), at a constant **1**/DBU = 1:10,000 ratio. Lowering the Li amount from 1.0 mmol to 0.5 and 0.25 mmol did not significantly affect the reaction results, with yields of 56 and 59 %, respectively. Using a **1**/DBU ratio of 1:20,000 and **1**/LiOTf = 1:500, formate was obtained in 24 % yield relative to DBU, with TON = 4729 (entry 19).

The effect of temperature increase was then tested, switching from 100 to 120 °C, initially on 24 h runs, at a constant LiOTf/DBU = 1:40 ratio and **1**/DBU ratios varying from 1:10,000 to 1:50,000 (entries 20–22). The best result was obtained with **1**/DBU = 1:20,000, with a yield of 83 % and TON = 16469. Next, the effect of increased gas mixture total pressure from 60 to 80 bar was tested, at LiOTf/DBU = 1:40 ratio and **1**/DBU ratios varying from 1:20,000 to 1:100,000 (entries 23–27), at reaction times ranging from 1 to 96 h. Under these optimized

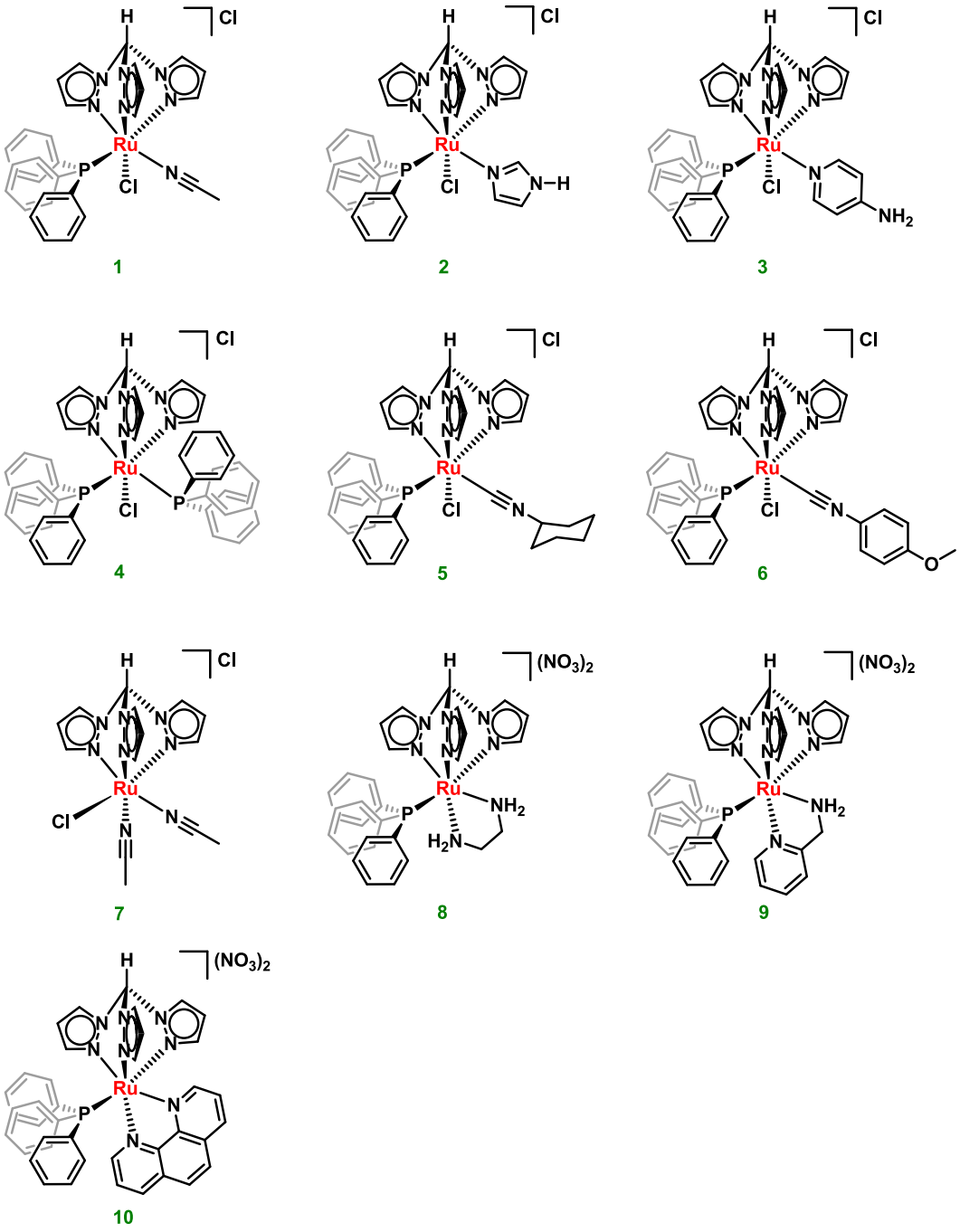

Fig. 1. Chemical drawings of Ru-tris(pyrazolyl)methane complexes (**1**–**10**) tested in this study.

conditions, the best yield in formate (84 %) was obtained after 24 h using **1**/DBU = 1:20,000, **1**/LiOTf = 1:500, 120 °C, with a corresponding TON = 16,637 (entry 23). The highest TON = 54,169 was instead observed at **1**/DBU = 1:100,000, **1**/LiOTf = 1:2500 and 120 °C after 96 h, with a formate yield of 55 %. The catalytic results are summarized in Table 3 and selected data are visualized as bar graph in Fig. 5.

An additional run at 1 h (entry 24) under the optimized conditions used for entry 23, allowed to obtain the value of initial TOF_{1h} = 5940 h^{-1} with a yield of 30 %, suggesting a fast reaction already in the first hour of the experiment. Finally, two proof-of-concept experiments were run to evaluate catalyst recyclability. In the first experiments, using the conditions applied for entry 14 (Table 3), after the first run the autoclave was cooled to 10 °C, gas pressure was carefully released and replaced by nitrogen. A new aliquot of DBU (84 % of the amount used in run 1) was added through the inlet port without opening the autoclave, that was then re-pressurized with 80 bar CO_2/H_2 (1:1) and heated to 100 °C for 24 h (run 2). At the end of the reaction, formate was obtained in 81 % yield (TON = 4093), with only a slight decrease compared to run 1 (84 % yield). Thus, for the two consecutive runs under the described reaction conditions, it was possible to obtain an overall TON = 8338. The second experiment was carried out in a similar way, using the conditions applied for entry 20 (Table 3), *i.e.* at lower catalyst to base ratio and in the presence of LiOTf. For run 2, formate yield was confirmed at 87 % (TON = 8796), as in the case of run 1. An overall TON = 17,592 was therefore reached after the two consecutive runs under these conditions. These two experiments clearly demonstrate the possibility to efficiently recycle catalyst **1** for consecutive runs at low catalyst loadings, with and without the addition of the LiOTf co-catalyst.

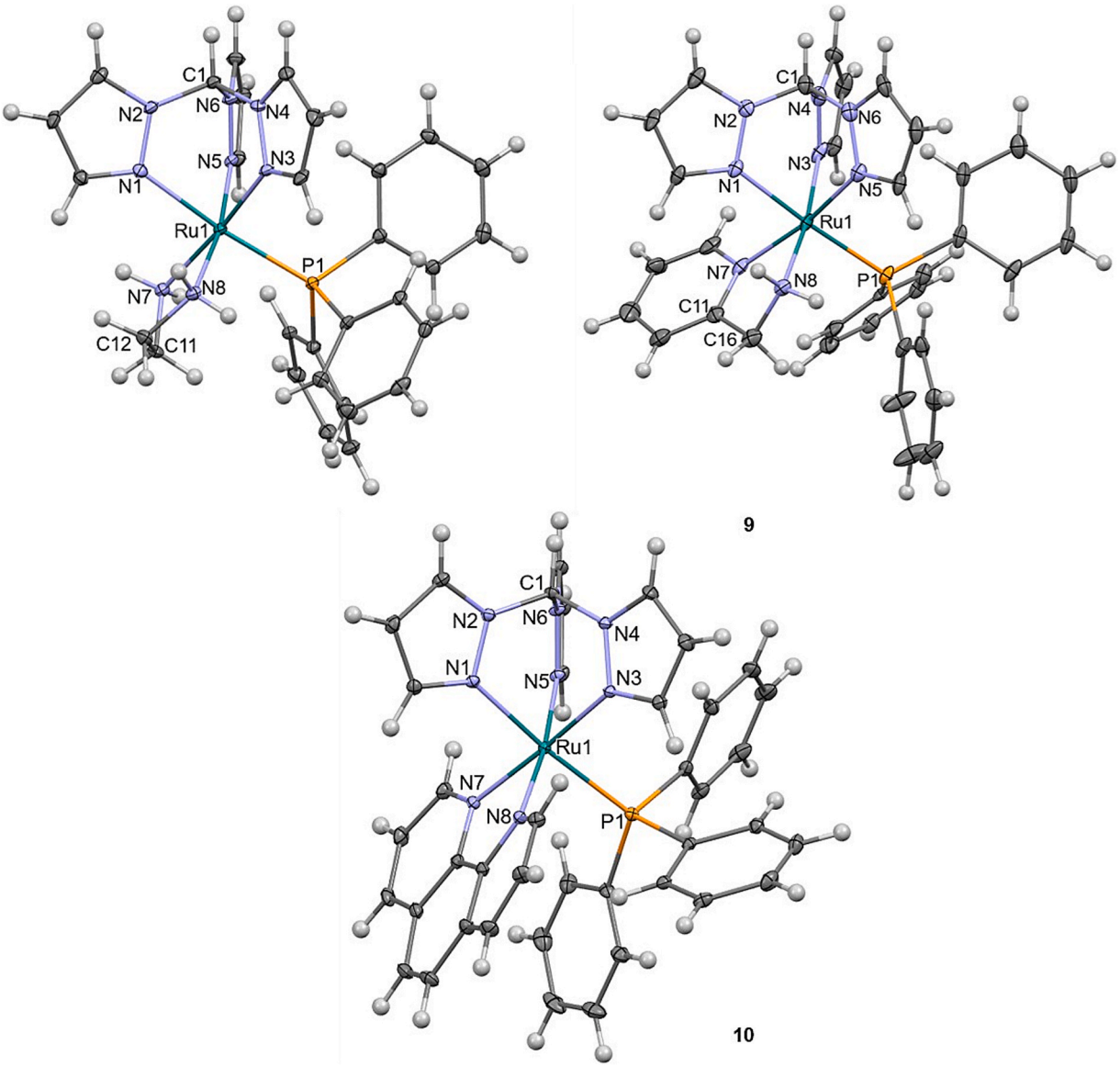

Fig. 2. Views of the X-ray crystal structures of complexes **8**–**10**. Displacement ellipsoids are at the 30% probability level.

2.3. Mechanistic studies

Due to the close structural similarity of complexes **1**–**10**, we reasoned that the mechanism of pre-catalyst activation could be common to most complexes, thus worth being investigated in detail. The mechanism of pre-catalyst activation was studied for the most active **1** and **4** by NMR spectroscopy. In the first series of experiments (Figs. S61 and S62), complex **4** (10 mg) was dissolved in THF-d_8 under nitrogen at room temperature. ^{1}H and ^{31}P{^{1}H} NMR spectra were collected, then isopropanol (10 equiv.) was added. Next, DBU (5 equiv. to **4**) was added to the mixture, NMR spectra were collected, then the NMR tube was placed in an oil bath set at 60 °C for 1 h. Whereas no changes were observed before heating, and only the singlet at 39.3 ppm due to **4** was observed in the ^{31}P{^{1}H} NMR spectra, after 1 h at 60 °C new signals appeared. In particular, the presence of free PPh_3 was observed at –6.4 ppm, suggesting ligand exchange between PPh_3 and solvent(s), leading to a mixture of four different species, characterized by broad singlets at 49.6, 49.9, 50.7 and 52.3 ppm. This reactivity can be expected upon substitution of one PPh_3 ligand with a solvent molecule, to give initially a species such as [RuCl(κ^3-tpm)(solv)(PPh_3)]Cl (solv = THF-d_8 or ^{i}PrOH). Then, the presence of a strong base (DBU) can deprotonate coordinated ^{i}PrOH, giving complexes such as [RuCl(κ^3-tpm)(^{i}PrO)(PPh_3)] and/or

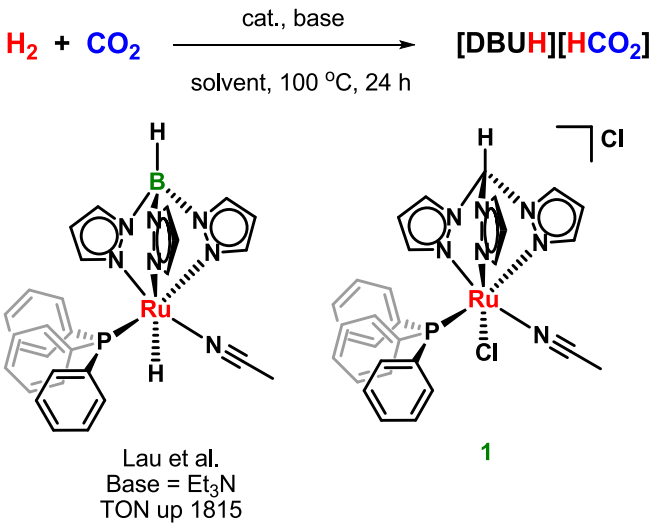

Scheme 1. General scheme and standard conditions for CO_2 hydrogenation tests. Drawings of Ru-tris(pyrazolyl)borate [TpRuH(PPh_3)(CH_3CN)] complex [26] and Ru-tris(pyrazolyl)methane complex **1** are shown for comparison.

Table 2
CO_2 hydrogenation catalyzed by complexes **1**–**10**, in different solvents and with different bases.[a]

Entry	Catalyst	Base	Solvent	Cat./Base ratio	TON[b]	Yield[c] (%)
1	**1**	NEt_3	THF	1/1104	0	0
2	**1**	NEt_3	THF/H_2O	1/1104	0	0
3	**1**	NEt_3	Toluene	1/1104	0	0
4	**1**	NEt_3	MeOH	1/1104	84	5
5	**1**	DBU	MeOH	1/1000	167	17
6	**1**	DBU	^{i}PrOH	1/1000	1004	≥99
7	**1**	KO^{t}Bu	^{i}PrOH	1/1000	175	17
8	**2**	DBU	^{i}PrOH	1/1000	932	93
9	**3**	DBU	^{i}PrOH	1/1000	932	93
10	**4**	DBU	MeOH	1/1000	183	18
11	**4**	DBU	^{i}PrOH	1/1000	910	90
12	**5**	DBU	^{i}PrOH	1/1000	819	82
13	**6**	DBU	^{i}PrOH	1/1000	628	63
14	**7**	DBU	^{i}PrOH	1/1000	530	53
15	**8**	DBU	^{i}PrOH	1/1000	418	42
16	**9**	DBU	^{i}PrOH	1/1000	89	9
17	**10**	DBU	^{i}PrOH	1/1000	11	1

[a] Reaction conditions: catalyst, 10–13 μmol; Base, 10–14 mmol; solvent, 6 (entries 5–15) or 20 mL (entries 1–4); H_2/CO_2 (1:1) 60 bar total pressure; 100 °C, 24 h.
[b] TON = (mmol formate)/(mmol catalyst);
[c] Yield = [(mmol formate)/(mmol DBU)] x 100. The amount of formate was calculated from the integration of the corresponding ^{1}H NMR signal in D_2O against an internal standard (DMF). All experiments were repeated at least twice to check for reproducibility, average error ca. 6 %.

[Ru(κ^3-tpm)(solv)(^{i}PrO)(PPh_3)]$^+$. After 24 h at 60 °C, only two singlets out of the four observed after 1 h were still present, namely at 49.9 and 50.7 ppm, in addition to unreacted **4** and free PPh_3. The reactivity pattern did not change significantly in a second set of experiments, run under the same conditions except for decreasing the amount and ratio between DBU and ^{i}PrOH (2 equiv. each to **4**), as shown in Figs. S63 and S64.

In the second series of experiments, a similar sequence of ^{1}H and ^{31}P{^{1}H} NMR experiments was run with **1** instead of **4** (Figs. S65 and S66). Thus, complex **1** was initially dissolved in THF-d_8, recording the first spectra, then 2 equiv. of ^{i}PrOH were added and spectra were recorded, followed by the addition of 2 equiv. of DBU, recording the final set of spectra at 25 °C. As in the case of **4**, reactivity of **1** with solvent and base was observed only upon heating the reaction mixture. After 1 h heating to 60 °C, the singlet due to unreacted **1** at 48.1 ppm was present together with three new broad singlets at the same chemical shift values previously observed with **4**, namely 49.6, 49.9, 50.7 ppm. After 24 h heating to 60 °C, the pattern simplified to the two singlets at 49.9 (major) and 50.7 ppm, with a decrease in intensity of the signal due to **1**. In the corresponding ^{1}H NMR spectra, it was observed that the initial signal at 2.16 ppm due to coordinated acetonitrile in **1** disappeared already after 1 h upon heating in the presence of isopropanol and base, and a new signal at 1.95 ppm, that was attributed to free acetonitrile appeared. Acetonitrile substitution by isopropanol in **1** upon heating was further confirmed in a third experiment with **1**, ^{i}PrOH and the same sequence described above but in the absence of DBU (Figs. S67, S68). The ^{31}P{^{1}H} NMR spectrum recorded after 1 h at 60 °C showed a single broad singlet at 49.6 ppm, that is thus assigned to [RuCl(κ^3-tpm)(^{i}PrOH)(PPh_3)]Cl (**11**). Interestingly, in none of these experiments signals at negative chemical shift values in ^{1}H NMR spectra, that could be expected upon Ru-H bond formation derived by a transfer hydrogenation mechanism in the presence of ^{i}PrOH/base, were observed. In turn, this suggests that such a mechanism may not take place for these complexes under the applied conditions.

By comparing the NMR experiments, we conclude that both pre-catalysts **1** and **4** undergo activation by (reversible) ligand substitution, *i.e.* by release of either MeCN or a PPh_3 ligand, respectively, to generate the same intermediate **11** upon ^{i}PrOH coordination. This step may then be followed by ^{i}PrOH deprotonation by DBU, giving [RuCl(κ^3-tpm)(^{i}PrO)(PPh_3)] (**12**), which can further react with ^{i}PrOH or THF to give a putative solvento species such as [Ru(κ^3-tpm)(solv)(^{i}PrO)(PPh_3)]Cl (**13**). Attempts to synthesize and isolate pure samples of **11**–**13** failed due to decomposition upon workup. For this reason, it was not possible to conclusively assign the remaining ^{31}P{^{1}H} NMR signals at 49.9 and 50.7 ppm observed during the experiments described above. The proposed pre-catalysts activation pathway, based on NMR experiments and in the absence of CO_2 and H_2, is shown in Scheme 2.

A final experiment was carried out to assess the possible formation of

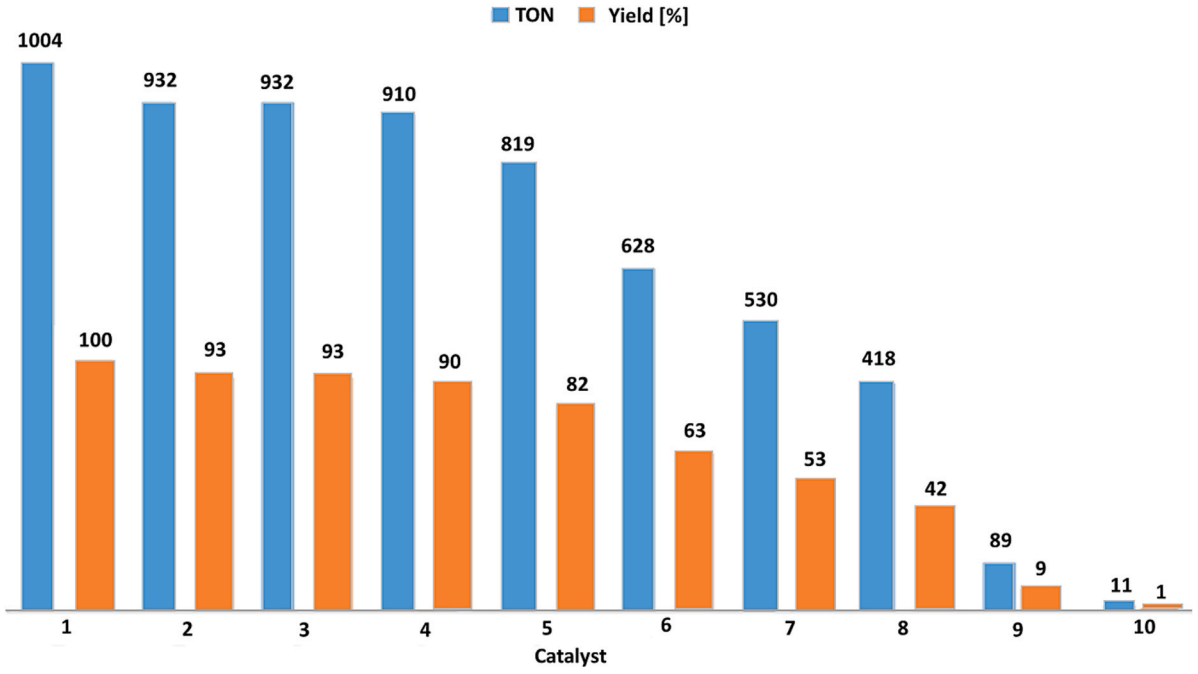

Fig. 3. Screening of the activity of Ru complexes **1**–**10** in CO_2 hydrogenation. Reaction conditions: see Table 2 footnote. TON and yield bar scales are independent for better clarity.

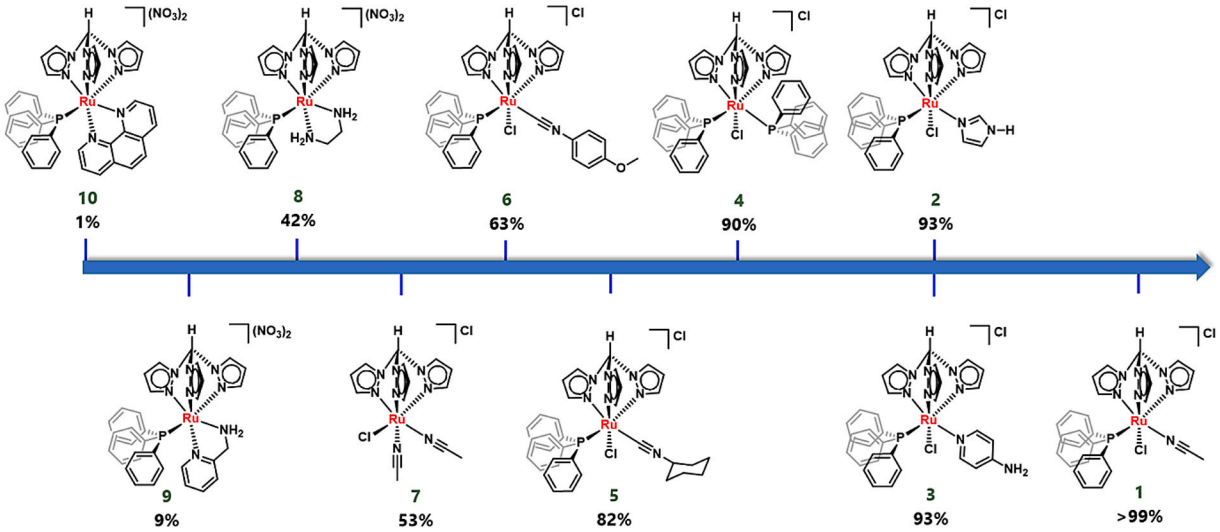

Fig. 4. Ru-tris(pyrazolyl)methane complexes **1**–**10** activity growing trend in formate yields (%) at catalyst/DBU = 1:1000, 100 °C, 24 h.

Ru hydrido complexes upon H_2 activation by the metal center. To a screw-cap NMR tube containing a solution of **1**, ^{i}PrOH (2 equiv.), DBU (2 equiv.) in THF-d_8, initially placed in an ice bath to avoid solvent evaporation, H_2 gas (1 bar) was bubbled through for 15 min. The tube was shaken and let to warm to room temperature. $^{31}P\{^{1}H\}$ NMR analysis showed as expected the appearance of signals due to **11** and **12**. The NMR tube was then heated to 60 °C for 12 h. After this time, the ^{1}H NMR spectrum (Fig. S69) showed two new doublets in the negative chemical shift range at −13.65 ppm (d, $^{2}J_{PH}$ = 31 Hz) and at −14.53 ppm (d, $^{2}J_{PH}$ = 27 Hz), accompanied by new singlets at 74.5 and 77.1 ppm in the corresponding $^{31}P\{^{1}H\}$ NMR spectrum (Fig. S70), indicative of the formation of two monohydrido Ru complexes, to which we attribute putative formulas [RuH(κ^3-tpm)(^{i}PrOH)(PPh$_3$)]$^+$ (**14**) and [RuH(κ^3-tpm)(^{i}PrO)(PPh$_3$)] (**15**).

In order to understand the key mechanistic aspects of the catalytic reaction and confirm the proposed pre-activation pathway, a detailed Density Functional Theory (DFT) analysis of the reaction pathway involved in the catalytic mechanism in the presence of **1** was carried out at M062X-DFT level of theory with the inclusion of the dispersion forces. The calculations were performed considering solvent effects using the Conductor-like Polarizable Continuum Model (CPCM) for 2-propanol, the same solvent used in the experimental tests. Initially, the structure of the cationic ruthenium octahedral complex [RuCl(κ^3-tpm)(PPh$_3$)(MeCN)]$^+$ (**1**, **A**$^+$ in the calculations) featuring a triphenylphosphine, a chloride, an acetonitrile and a κ^3-tris(pyrazolyl)methane ligands was optimized. Next, the free energy costs associated with the removal of each of the ancillary ligands from the coordination sphere of the metal in **A**$^+$ were separately calculated. The structures of the potential pentacoordinated intermediates, obtained by alternatively removing CH_3CN, Cl^- or PPh_3 from **A**$^+$ were optimized. The removal of the coordinated acetonitrile was estimated to be endergonic by + 10.8 kcal mol^{-1}, whereas chloride or triphenylphosphine dissociation would cost + 26.4 and + 21.0 kcal mol^{-1}, respectively. Thus, the most favorable, least energetically demanding process is the dissociation of MeCN to give [RuCl(κ^3-tpm)(PPh$_3$)]$^+$ (**B**$^+$). As the experimental tests were run in 2-propanol, the possible coordination of the solvent to **B**$^+$ was then calculated. This step provides [RuCl(κ^3-tpm)(PPh$_3$)(κ^1*O*-^{i}PrOH)]$^+$ (**11**, **C**$^+$ in calculations) with an estimated free energy gain of −8.5 kcal mol^{-1}, in line with the experimental findings described above. The calculated structures of **A**$^+$, **B**$^+$ and **C**$^+$ are shown in Fig. 6.

At this point, in the real system the coordination of H_2 to the metal center should occur. This step generally leads to a Ru(η^2-H$_2$) intermediate evolving further to Ru-H species that in turn interact with CO_2. Different options were considered, depending on which of the ancillary ligands in **C**$^+$ could be more favorably removed. Direct ligand exchange of Cl^- with H_2 would give the bis(cationic) complex [Ru(η^2-H$_2$)(κ^3-tpm)(PPh$_3$)(κ^1*O*-^{i}PrOH)]$^{2+}$ (**D**$^{2+}$), but this process was discarded being highly energy-demanding, with a free energy cost of +28.1 kcal mol^{-1}. A possible alternative pathway was considered, where at first the acidic proton of the 2-propanol ligand in **C**$^+$ interacts with DBU, giving adduct **E**$^+$ that features a hydrogen bonding between the 2-propanol proton and the N5 atom of the DBU moiety (H-N5 distance of 1.63 Å). From an energy viewpoint, the formation of the adduct **E**$^+$ was estimated to be exergonic by −2.1 kcal mol^{-1}. The complete deprotonation of the coordinated 2-propanol by DBU from **E**$^+$ to afford the neutral intermediate [RuCl(κ^3-tpm)(PPh$_3$)(κ^1*O*-^{i}PrO)] (**11**, **F** in calculations) was estimated to be endergonic by +9.8 kcal mol^{-1}, with shortening of the Ru-O bond by *ca.* 0.1 Å. At this stage, one of the ligands may be displaced leaving a free coordination site for the interaction with the H_2 molecule. By the assistance of DBUH$^+$, generated in the previous step from the deprotonation of the coordinated 2-propanol, chloride can be released and the new free coordination site can be occupied by H_2 in a η^2-coordination fashion, resulting in the formation of the intermediate [Ru(η^2-H$_2$)(κ^3-tpm)(PPh$_3$)(κ^1*O*-^{i}PrO)]$^+$ (**G**$^+$) and [DBUH]$^+$Cl$^-$ salt. The free energy cost for this step was estimated as +9.2 kcal mol^{-1}. H_2 coordination to the metal center provides the appearance of a new peak in the calculated infrared spectrum at 3269 cm^{-1}, associated with H-H stretching. The calculated structures of **E**$^+$, **F** and **G**$^+$ are shown in Fig. 7.

Once **G**$^+$ was formed, two possible pathways were considered for the heterolytic activation of the (η^2-H$_2$) ligand. In the first one, the isopropoxide ligand acted as a base to convey intramolecular deprotonation affording the Ru-hydrido species [RuH(κ^3-tpm)(PPh$_3$)

Table 3
CO_2 hydrogenation in the presence of complexes **1**, **4, 6** and **7** under various conditions of catalyst concentration, temperature, pressure, time and addition of LiOTf.[a]

Entry	Catalyst	Cat./Base ratio	Cat./ LiOTf	Temp. [°C]	TON[b]	Yield[c] (%)
1	**4**	1/1000	–	100	910	91
2	**4**	1/2000	–	100	1738	87
3	**4**	1/2000	1/200	100	1532	76
4	**4**	1/5000	–	100	3427	68
5	**4**	1/5000	1/500	100	2920	58
6	**4**	1/5000	1/250	100	2818	56
7	**4**	1/10000	–	100	3362	33
8	**6**	1/1000	–	100	628	63
9[d]	**6**	1/1000	–	100	741	74
10[d]	**6**	1/1000	1/100	100	816	81
11	**7**	1/1000	1/100	100	946	94
12	**1**	1/1000	–	100	1004	≥99
13	**1**	1/2000	–	100	2008	≥99
14	**1**	1/5000	–	100	4245	84
15	**1**	1/10000	–	100	3436	34
16	**1**	1/10000	1/1000	100	5857	58
17	**1**	1/10000	1/500	100	5654	56
18	**1**	1/10000	1/250	100	5965	59
19	**1**	1/20000	1/500	100	4729	24
20	**1**	1/10000	1/250	120	8796	87
21	**1**	1/20000	1/500	120	16,469	83
22	**1**	1/50000	1/1250	120	15,241	31
23[e]	**1**	1/20000	1/500	120	16,637	84
24[e,f]	**1**	1/20000	1/500	120	5940	30
25[c]	**1**	1/50000	1/1250	120	20,543	42
26[e,g]	**1**	1/50000	1/1250	120	35,401	72
27[e,g]	**1**	1/100000	1/2500	120	54,169	55

[a] Reaction conditions: catalyst 1–10 μmol; DBU, 10 mmol; LiOTf (where present), 40–400 μmol; ^{i}PrOH, 6 mL; H_2/CO_2 (1:1) 60 bar total pressure; 24 h. All experiments were repeated at least twice to check for reproducibility, average error ca. 6 %.
[b] TON = (mmol formate)/(mmol catalyst);
[c] Yield = [(mmol formate)/(mmol DBU)] x 100. The amount of formate was calculated from the integration of the corresponding ^{1}H NMR signal in D_2O against an internal standard (DMF).
[d] 48 h.
[e] 80 bar.
[f] 1 h.
[g] 96 h.

(κ^1*O*-^{i}PrOH)]$^+$ (**H**$^+$). A transition State **TS**$_{\mathbf{G+/H+}}$ was computationally detected with a free energy barrier of 7.3 kcal mol^{-1}. In **TS**$_{\mathbf{G+/H+}}$, the O—H distance is largely shortened, up to 1.42 Å, compared to the starting value of 2.74 Å, while the H-H distance is 0.15 Å longer compared to the value in **G**$^+$. The nature of the transition state was confirmed by the detection of a single imaginary frequency at −1278 cm^{-1}, associated with the shortening of the O—H distance and the weakening of the H-H bond. After **TS**$_{\mathbf{G+/H+}}$, the system evolves toward **H**$^+$, with a large free energy gain of −25.1 kcal mol^{-1}. The total free energy for the conversion of **G**$^+$ to **H**$^+$ was estimated as −17.8 kcal mol^{-1}. In the second pathway, intermolecular deprotonation of the coordinated H_2 in **G**$^+$ by external DBU was considered as an alternative, to give a putative [RuH(κ^3-tpm)(PPh$_3$)(κ^1*O*-^{i}PrO)] complex. This reaction would be associated with a free energy gain of only −7.8 kcal mol^{-1}, less favorable compared to intramolecular deprotonation (−17.8 kcal mol^{-1}). The intermolecular pathway is associated with an estimated energy barrier of *ca.* 5 kcal mol^{-1}, that is comparable to the value obtained for the intramolecular process. Based on these findings, the formation of **H**$^+$ by intramolecular dihydrogen ligand deprotonation should be preferred. The optimized structures of transition state **TS**$_{\mathbf{G+/H+}}$, and intermediate **H**$^+$ are shown in Fig. 8.

The newly formed hydride ligand in **H**$^+$ is then aptly positioned for an outer-sphere interaction with incoming CO_2 to give at first the adduct **I**$^+$, featuring a bent CO_2 molecule with the O1-C1-O2 angle reduced by 46° than in the free molecule. CO_2 activation allows a strong elongation of the pristine Ru-H bond (1.82 Å *vs.* 1.58 Å in **I**$^+$ and **H**$^+$, respectively) and a *quasi*-formed H-C1 bond at 1.20 Å. This CO_2 activation causes the appearance of a calculated IR peak at 1789 cm^{-1} assigned to the C-O stretching, suggesting an efficient charge transfer from the hydride to the terminal CO_2 oxygen atoms. The formation of adduct **I**$^+$ starting from separated **H**$^+$ and CO_2 was estimated to be endergonic by 13.1 kcal mol^{-1}. Interestingly, the presence of a hydrogen bond between the 2-propanol proton and the O2 atom of CO_2 in **I**$^+$ was observed, with a distance of 1.67 Å, similar to what proposed by Lau and co-workers for CO_2 hydrogenation using in the presence of [TpRuH(PPh$_3$)(CH$_3$CN)] as a catalyst [26]. The intermediate **I**$^+$ releases HCOOH in the presence of the external base (DBU), to give the formate end product. This reaction serves as the thermodynamic driving force for CO_2 hydrogenation reactions in the presence of a base. Relaxed scan from **I**$^+$ along the C-H and O-H reaction coordinate for the formation of formic acid provides an estimation of the energy barrier of 8.2 kcal mol^{-1} leading to the transition state **TS**$_{\mathbf{I+/J+}}$. This state then evolves into the pentacoordinated

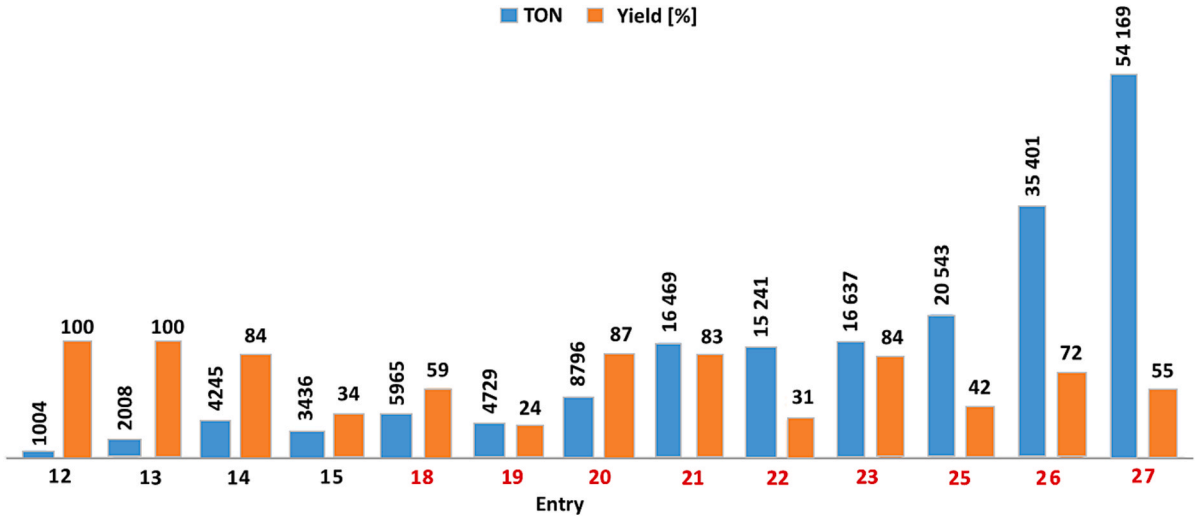

Fig. 5. Selected data for CO_2 hydrogenation in the presence of **1** at different catalyst/base ratios under various conditions. Reaction conditions: see Table 3 footnote. Entry numbers in red belong to runs with added LiOTf co-catalyst. TON and yield bar scales are independent for better clarity. (For interpretation of the references to colour in this figure legend, the reader is referred to the web version of this article.)

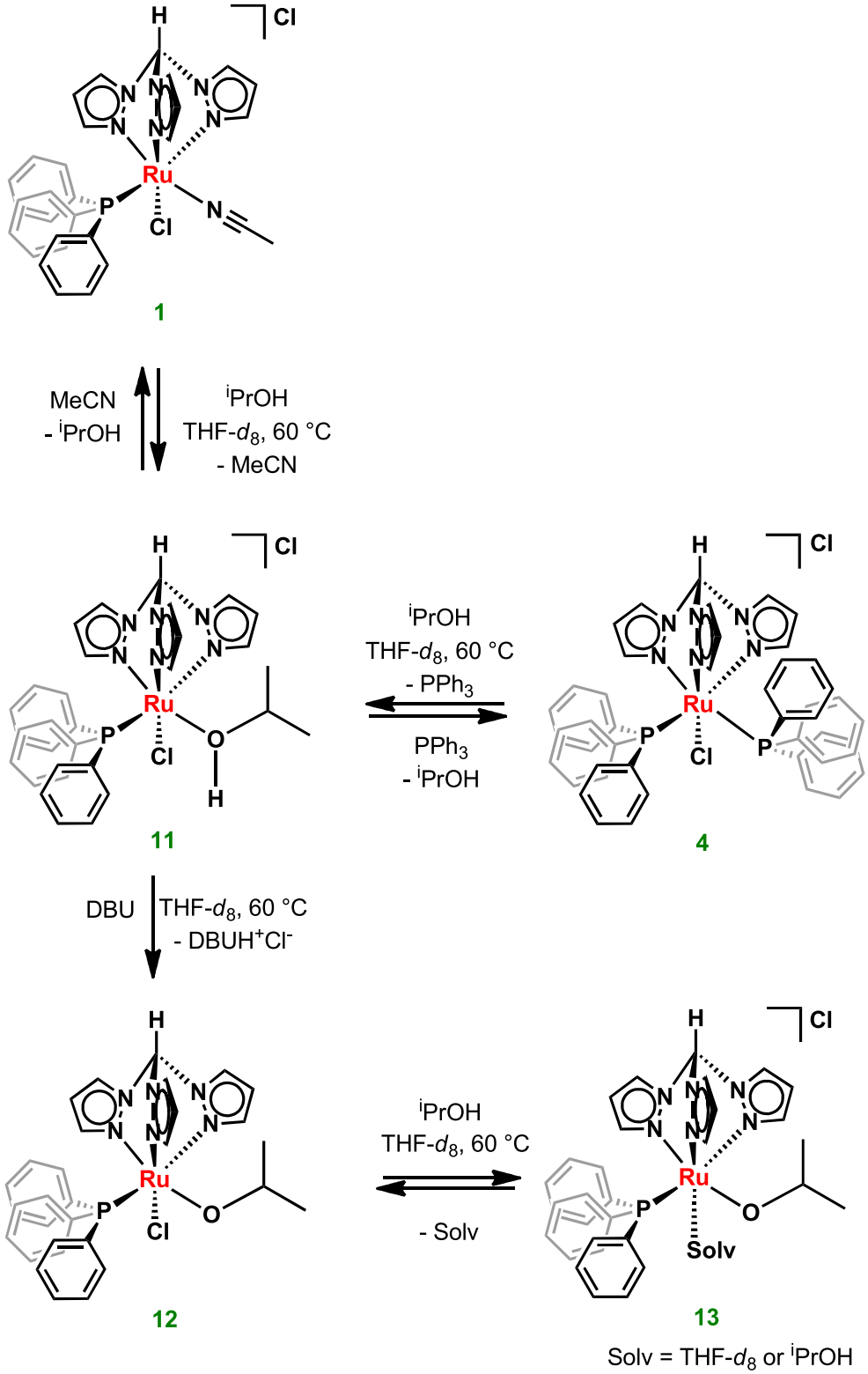

Scheme 2. Proposed pathway for pre-activation of **1** and **4** in the presence of ^{i}PrOH and DBU.

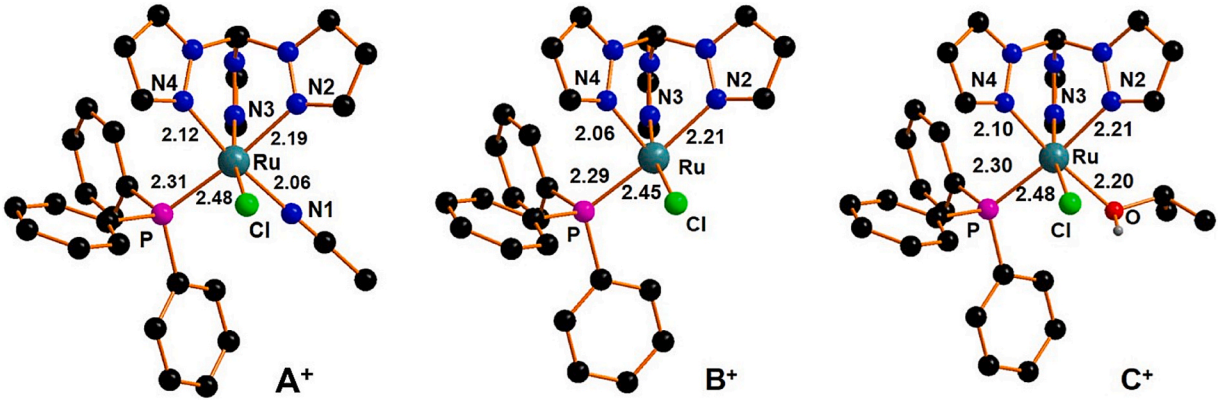

Fig. 6. Optimized structures of complex $\mathbf{A}^+$ and intermediates $\mathbf{B}^+$ and $\mathbf{C}^+$. Hydrogen atoms were omitted for clarity except for the OH proton of coordinated 2-propanol in $\mathbf{C}^+$.

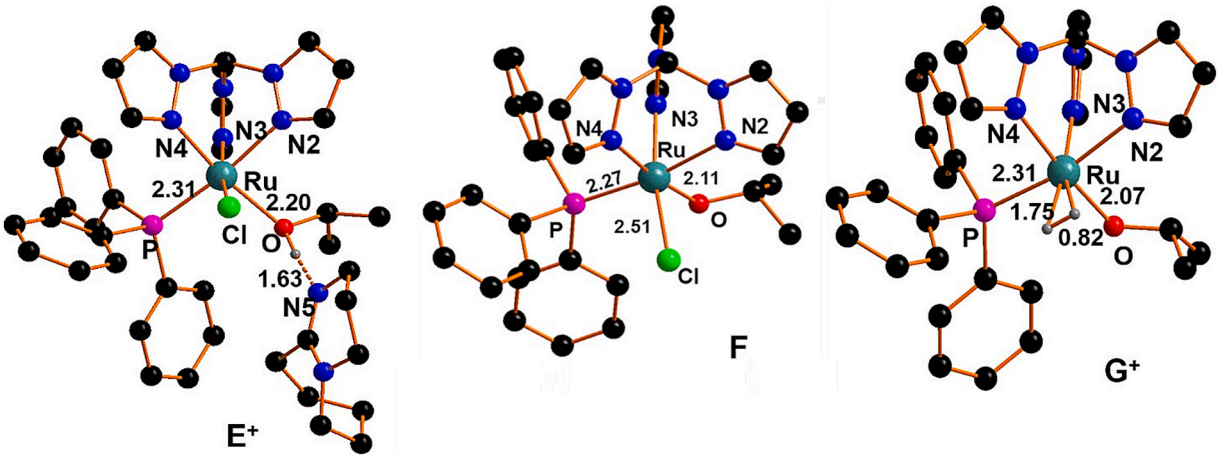

Fig. 7. Optimized structures of intermediates $\mathbf{E}^+$, **F** and $\mathbf{G}^+$. Hydrogen atoms were omitted for clarity except for the OH proton of coordinated 2-propanol in $\mathbf{E}^+$.

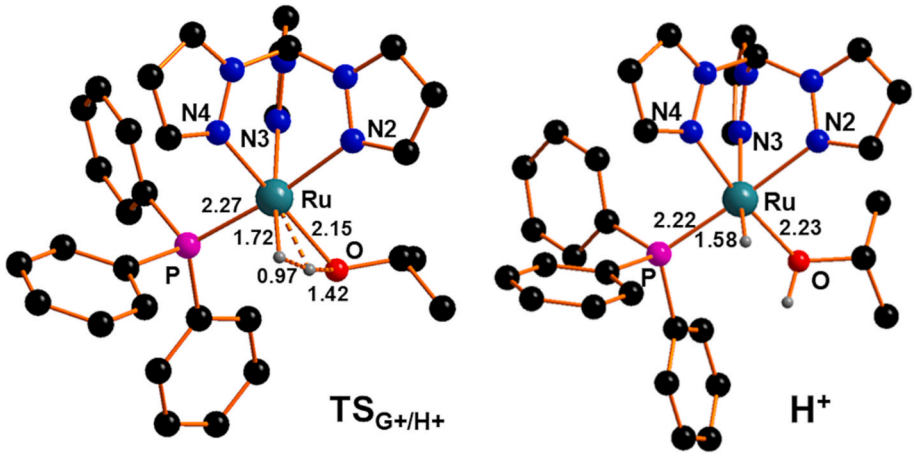

Fig. 8. Optimized structures of transition state $\mathbf{TS}_{\mathbf{G+/H+}}$ and intermediate $\mathbf{H}^+$. Hydrogen atoms were omitted for clarity except for the H_2 ligand and the OH proton of coordinated 2-propanol.

species $[Ru(\kappa^3\text{-tpm})(PPh_3)(\kappa^1O\text{-}^i PrO)]^+$ ($\mathbf{J}^+$). The formation of $\mathbf{J}^+$ together with the ionic pair $[DBUH^+][HCOO^-]$ was associated with an overall free energy cost of only +2.3 kcal mol^{-1}. The optimized structures of the transition state $\mathbf{TS}_{\mathbf{H+/J+}}$ and the intermediates $\mathbf{I}^+$ and $\mathbf{J}^+$ are shown in Fig. 9.

Finally, the coordination of another H_2 molecule to $\mathbf{J}^+$ restores the intermediate $\mathbf{G}^+$ with a *quasi-null* free energy cost of only +0.7 kcal mol^{-1}, allowing the catalytic cycle to restart. The overall free energy for the entire process was calculated as −1.7 kcal mol^{-1}, well within reach under experimental conditions. The free energy pathway from $\mathbf{A}^+$ to $\mathbf{I}^+$ is shown in Fig. S72. Based on the combination of experimental data and DFT calculations, the proposed simplified catalytic cycle, following the initial pre-catalyst activation step, is shown in Scheme 3.

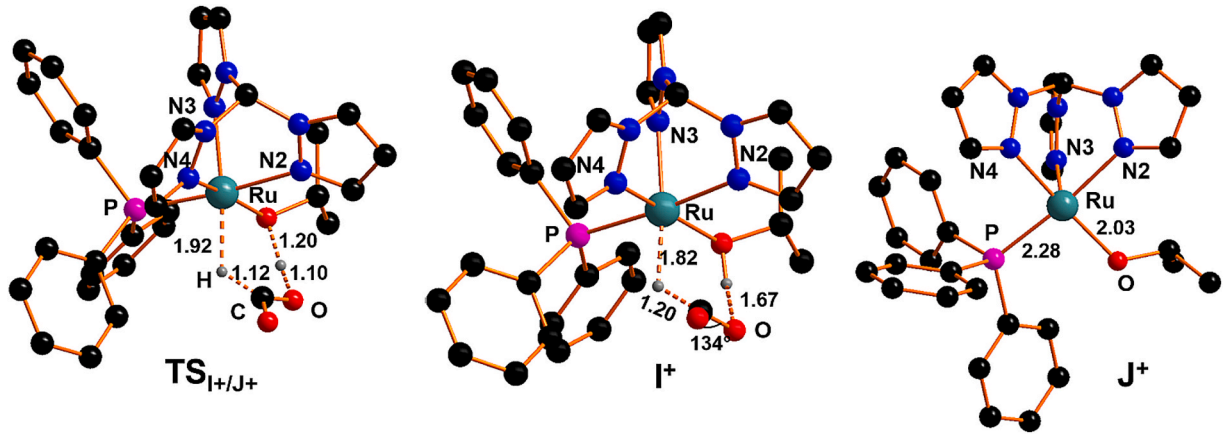

Fig. 9. Optimized structures of the transition state $\mathbf{TS}_{H+/J+}$ and the intermediates $\mathbf{I}^+$ and $\mathbf{J}^+$. Hydrogen atoms were omitted for clarity except for the H_2 ligand and the OH proton of coordinated 2-propanol.

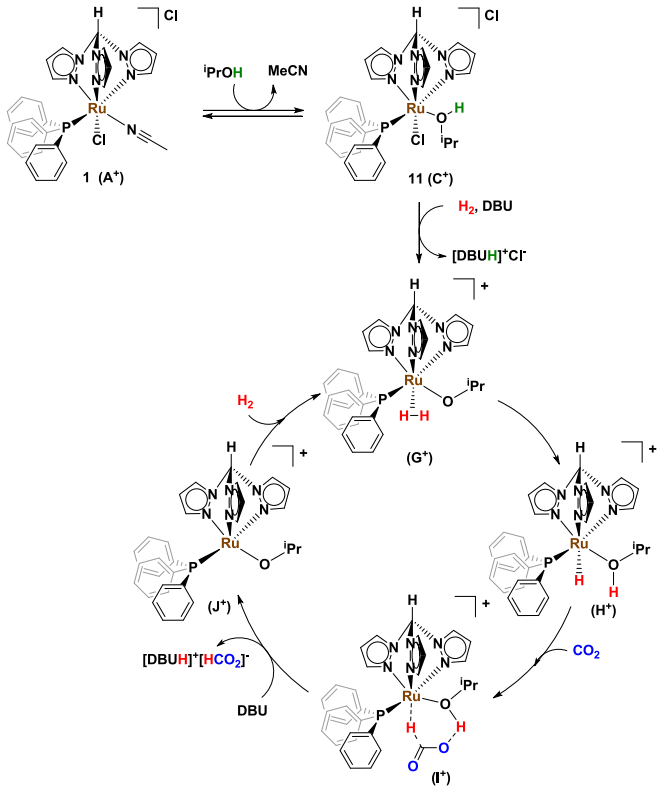

Scheme 3. Proposed simplified catalytic cycle for CO_2 hydrogenation to formate starting from pre-catalyst $\mathbf{A}^+$.

3. Conclusions

In conclusion, octahedral ruthenium(II) complexes bearing tris(pyrazolyl)methane as κ^3-capping ligand, with varying combinations of the three remaining ligands in the coordination sphere of the metal, were successfully tested for the first time as well-defined homogeneous catalysts for CO_2 hydrogenation to formate, in the presence of a base and a Li salt co-catalyst. Among the tested catalysts, complex [RuCl(κ^3-tpm)(PPh_3)(MeCN)]Cl (**1**) gave the highest activity, reaching TON >54,000 in single batch runs, at a catalyst loading of 0.001 mol% relative to the base and in the presence of LiOTf as co-catalyst. Mechanistic studies highlighted the role of the solvent (^{i}PrOH) and the base (DBU) in crucial steps of pre-catalyst activation and in the catalytic cycle. About the effect of lithium salt, in the absence of more conclusive experimental evidence, it is plausible that, together with a possible role in the catalytic mechanism as previously described for other systems [10g],[35],[36], it may also work in the pre-catalyst activation step as chloride scavenger. The role of alkali metal salts as halide scavengers for Ru(II) coordination compounds has been widely reported in the literature [37]. Finally, proof-of-concept experiments showed that the catalyst solution obtained from **1** can be efficiently recycled for consecutive runs, without minor or no loss of activity. In summary, the present results demonstrate the potential of tris(pyrazolyl)methane complexes in previously neglected catalytic reactions of high current interest, and pave the way for further studies in other CO_2 reduction processes, that are currently ongoing in our laboratories.

4. Experimental section

4.1. Synthesis and characterization of Ru complexes 6, 8–10

[RuCl(κ^3-tpm)(PPh_3)(CNC(CH)$_4$COCH$_3$)]Cl (**6**)

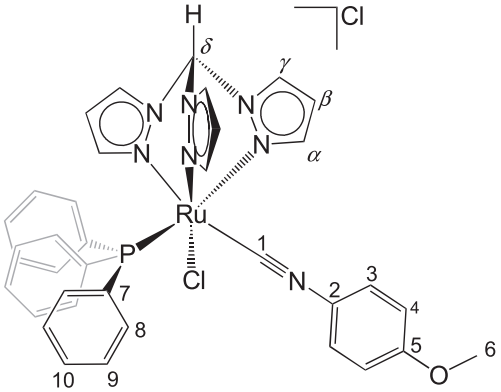

A solution of **4** (150 mg, 0.165 mmol) and 4-methoxyphenyl isocyanide, CNC(CH)$_4$COCH$_3$ (23 mg, 0.17 mmol) in 10 mL of ethanol was heated at reflux for 5 h. Hence, the volatiles were evaporated under reduced pressure, and the solid residue was washed with diethyl ether (25 mL) and then dried under vacuum. Yellow solid, yield 126 mg (98 %). The title compound was also prepared in comparable efficiency using **1** instead of **4** as starting material, following a similar synthetic protocol. Anal. calcd. for $C_{36}H_{32}Cl_2N_7OPRu$: C, 55.32; H, 4.13; N, 12.54; Cl, 9.07. Found: C, 55.16; H, 4.02; N, 12.36; Cl, 9.18. IR (solid state): $\tilde{\nu}$/cm^{-1} = 3092 w, 2133 s (C^{1}N), 1603 w, 1505 s, 1481 w, 1487 m, 1435 m, 1406 m, 1251 s, 1221 w, 1185 w, 1166 w, 1086 s, 1048 m, 1022 w, 990 w, 983 w, 896 w, 834 s, 791 s, 762 s, 742 s, 699 s, 690 s. ^{1}H NMR ($CDCl_3$): δ/ppm = 12.39 (s, 1H, C$^\delta$H); 8.94, 8.79, 8.65 (d-br, 3H, C$^\gamma$H); 8.13, 6.82, 6.14 (d-br, 3H, C$^\alpha$H); 7.51 (t-br, 6H, C^8); 7.40 (t, 3H, $^3J_{HH}$ =

7.45 Hz, C^{10}); 7.30 (t-br, 6H, $^3J_{HH}$ = 7.88 Hz, C^9); 7.10 (d, 2H, $^3J_{HH}$ = 8.40 Hz, C^4); 6.85 (d, 2H, $^3J_{HH}$ = 8.43 Hz, C^3); 6.39, 6.11, 5.94 (t-br, 3H, $C^{\beta}H$); 3.82 (s, 2H, C^6H). $^{13}C\{^1H\}$ NMR ($CDCl_3$): δ/ppm = 159.4 (C^5); 147.4, 145.9, 145.0 (C^{α}); 135.9, 134.5, 133.4 (C^{γ}); 134.2 (d, $^2J_{CP}$ = 9.6 Hz, C^8); 132.4 (d, $^1J_{CP}$ = 45.4 Hz, C^7); 130.4 (C^{10}); 128.5 (d, $^3J_{CP}$ = 9.6 Hz, C^9); 127.4 (C^4); 122.4 (C^2); 114.7 (C^3); 108.3, 108.1, 108.0 (C^{β}); 74.2 (C^{δ}); 55.7 (C^6). $^{31}P\{^1H\}$ NMR ($CDCl_3$): δ/ppm = 47.6. Labeling refers to carbon atoms as in the molecular drawing shown above.

[Ru(κ^3*N*-tpm)(κ^2*N*-$NH_2CH_2CH_2NH_2$)(PPh_3)][NO_3]$_2$ (**8**)

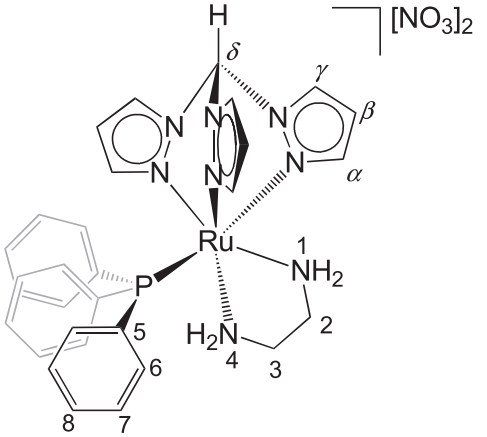

A mixture of **4** (100 mg, 0.11 mmol), ethylenediamine (7.35 mL, 0.11 mmol) and $AgNO_3$ (37 mg, 0.22 mmol) in ethanol (7 mL) was refluxed overnight. After cooling to room temperature, the final mixture was filtered through celite, and the solvent evaporated under reduced pressure. The crude product was redissolved in the minimum volume of dichloromethane, and this solution was filtered on celite. The volatiles were then evaporated under reduced pressure. The obtained powder was dispersed in THF (ca. 10 mL) and left stirring for 1 h. The final mixture was filtered, and the solid isolated was washed with diethyl ether (2 x 10 mL) and then dried under vacuum. White solid, yield 80 mg (96 %). Anal. calcd. for $C_{30}H_{42}N_{10}O_6PRu$: C, 46.75; H, 5.49; N, 18.17. Found: C, 46.63; H, 5.42; N, 18.06. IR (solid state): $\tilde{u}/cm^{-1}$ = 3670 w, 3329 w, 3298 w, 3277 w, 3241 w, 3155 w, 3113 w, 2984 m, 2972 m, 2902 m, 1613 m (δ_{NH}), 1518 w, 1479 w, 1434 m, 1360 s ($\tilde{u}_{NO3}$), 1317 s, 1288 m, 1253 m, 1233 m, 1187 m, 1152 w, 1089 s, 1058 s, 890 w, 855 m, 827 m, 791 m, 751 s, 741 s, 699 s, 610 m, 606 m, 530 s, 506 s, 459 m. ^1H NMR (CD_3OD): δ/ppm = 9.80 (s, 1H, $C^{\delta}H$); 8.52 (d, 1H, $^3J_{HH}$ = 2.7 Hz, $C^{\gamma}H$); 8.50 (d, 2H, $^3J_{HH}$ = 3.0 Hz, $C^{\gamma}H$); 8.32 (d, 1H, $^3J_{HH}$ = 2.3 Hz, $C^{\alpha}H$); 7.52 (m, 3H, C^8H); 7.48 (m, 6H, C^6H or C^7H); 7.06 (d, 2H, $^3J_{HH}$ = 2.3 Hz, $C^{\alpha}H$); 7.02 (m, 6H, C^6H or C^7H); 6.72 (t-br, 1H, $C^{\beta}H$); 6.35 (t, 2H, $^3J_{HH}$ = 2.9 Hz, $C^{\beta}H$); 4.50 (m, 2H, $N^1H + N^4H$); 3.73 (m, 2H, $N^1H + N^4H$); 2.87 (m, 2H, $C^2H + C^3H$); 2.55 (m, 2H, $C^2H + C^3H$). ^{13}C NMR (CD_3OD): δ/ppm = 158.0 ($2C^{\alpha}$); 155.8 (C^{α}); 145.4 ($2C^{\gamma}$); 144.4 (C^{γ}); 141.9 (d, $^2J_{CP}$ = 9.5 Hz, C^6); 140.3 (d, $^1J_{CP}$ = 40.6 Hz, C^5); 140.0 (C^7); 138.9 (d, $^3J_{CP}$ = 9.3 Hz, C^6); 118.2 ($2C^{\beta}$); 117.5 (C^{β}); 84.9 (C^{δ}); 54.18 ($C^2 + C^3$). $^{31}P\{^1H\}$ NMR (CD_3OD): δ/ppm = 55.1. ^1H NMR (D_2O): δ ppm = 9.47 (s, 1H, $C^{\delta}H$); 8.39 (d, 3H, $^3J_{HH}$ = 2.9 Hz, $C^{\gamma}H$); 8.18 (d, 1H, $^3J_{HH}$ = 2.3 Hz, $C^{\alpha}H$); 7.57 (t, 3H, $^3J_{HH}$ = 7.4 Hz, C^8H); 7.46 (t, 6H, $^3J_{HH}$ = 7.4 Hz, C^6H or C^7H); 7.07 (d, 2H, $^3J_{HH}$ = 2.2 Hz, $C^{\alpha}H$); 7.04 (m, 6H, C^6H or C^7H); 6.64 (t-br, 1H, $C^{\beta}H$); 6.27 (t, 2H, $^3J_{HH}$ = 2.9 Hz, $C^{\beta}H$); 4.23 (m, 2H, $N^1H + N^4H$); 3.66 (m, 2H, $N^1H + N^4H$); 2.91 (m, 2H, $C^2H + C^3H$); 2.60 (m, 2H, $C^2H + C^3H$). $^{31}P\{^1H\}$ NMR (D_2O): δ/ppm = 56.0. Labeling refers to carbon atoms as in the molecular drawing shown above. Crystals suitable for X-ray diffraction were collected by slow evaporation of the solvent from a methanol solution of **8**.

[Ru(κ^3*N*-tpm)(κ^2*N*-$C_5H_4NCH_2NH$)(PPh_3)][NO_3]$_2$ (**9**)

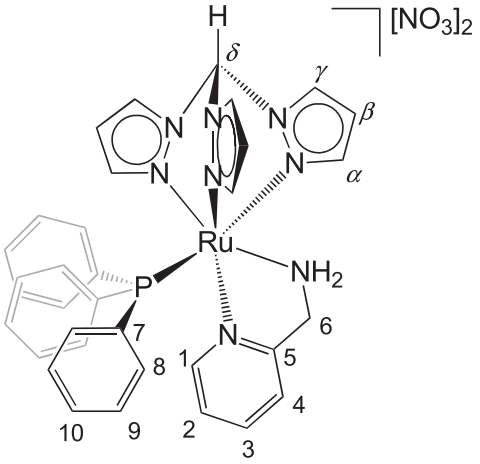

A mixture of **4** (100 mg, 0.11 mmol), 2-picolylamine (10.8 mL, 0.11 mmol) and $AgNO_3$ (37 mg, 0.22 mmol) in ethanol (7 mL) was refluxed for 6 h. The subsequent workup was performed following the procedure described for complex **8**. White solid, yield 84 mg (94 %). Anal. calcd. for $C_{34}H_{33}N_{10}O_6PRu$: C, 50.43; H, 4.11; N, 17.30. Found: C, 50.39; H, 4.01; N, 17.28. IR (solid state): $\tilde{u}/cm^{-1}$ = 3664 w, 3417 w, 3283 w, 3244 w, 3146 w, 3183 w, 2988 w, 2902 w, 1598 m (δ_{NH}), 1516 w, 1481 w, 1450 m, 1434 m, 1377 s ($\tilde{u}_{NO3}$), 1344 s ($\tilde{u}_{NO3}$), 1277 s, 1252 m, 1246 m, 1229 m, 1182 w, 1152 w, 1091 m, 1085 m, 857 m, 827 m, 781 s, 765 s, 752 s, 694 s, 614 m, 609 m, 529 s, 503 m. ^1H NMR ($CDCl_3$): δ/ppm = 11.20 (s, 1H, $C^{\delta}H$); 8.77, 8.54, 8.50 (d, 3H, $^3J_{HH}$ = 2.9 Hz, $C^{\gamma}H$); 7.88 (d, 1H, $^3J_{HH}$ = 5.7 Hz, C^1H); 7.78 (t-br, 1H, $^3J_{HH}$ = 7.7 Hz, C^3H); 7.44 (t-br, 3H, $^3J_{HH}$ = 7.3 Hz, $C^{10}H$); 7.39 (d, 1H, $^3J_{HH}$ = 8.5 Hz, C^4H); 7.27 (m, 6H, C^8H); 7.40, 7.34, 6.59 (d, 3H, $^3J_{HH}$ = 2.0 Hz, $C^{\alpha}H$); 7.16 (t-br, 1H, $^3J_{HH}$ = 6.5 Hz, C^2H); 6.67 (m, 6H, C^9H); 6.31, 6.25, 6.16 (t, 3H, $^3J_{HH}$ = 2.3 Hz, $C^{\beta}H$); 4.94–4.79 (m, 2H, NH_2); 4.48 (dd, 1H, $^2J_{HH}$ = 16.4 Hz, $^3J_{HH}$ = 5.1 Hz, C^6H); 3.17 (m, 1H, C^6H). $^{31}P\{^1H\}$ NMR ($CDCl_3$): δ/ppm = 52.8. ^1H NMR (CD_3OD): δ/ppm = 8.60, 8.56, 8.51 (dd, 3H, $^3J_{HH}$ = 2.9 Hz, $^4J_{HH}$ = 0.7 Hz, $C^{\gamma}H$); 8.06 (d-br, 1H, $^3J_{HH}$ = 5.8 Hz, C^1H); 7.96 (td, 1H, $^3J_{HH}$ = 7.7 Hz, $^4J_{HH}$ = 1.5 Hz, C^3H); 7.51 (m, 4H, $C^{10}H + C^4H$); 7.34 (m, 7H, $C^8H + C^2H$); 7.48, 7.10, 6.88 (d, 3H, $^3J_{HH}$ = 2.3 Hz, $C^{\alpha}H$); 6.77 (t-br, 6H, $^3J_{HH}$ = 8.9 Hz, C^9H); 6.54, 6.46, 6.42 (t, $^3J_{HH}$ = 2.9 Hz, 3H, $C^{\beta}H$); 4.27 (d, 1H, $^2J_{HH}$ = 16.53 Hz, C^6H); 3.33 (d, 1H, $^2J_{HH}$ = 16.50 Hz, C^6H); *NH_2 not observed.* ^{13}C NMR (CD_3OD): δ/ppm = 163.7 (C^5); 152.0 (C^1); 149.6, 148.1, 143.3 (C^{α}); 137.9 (C^3); 135.7, 135.5, 134.6 (C^{γ});132.7 (d, $^2J_{CP}$ = 9.7 Hz, C^8); 130.9 (d, $^1J_{CP}$ = 42.8 Hz, C^7); 130.8 (d, $^4J_{CP}$ = 2.2 Hz, C^{10}); 129.1 (d, $^3J_{CP}$ = 9.4 Hz, C^9); 125.1 (C^2); 122.1 (C^4H); 109.2, 108.9, 108.8 ($C^{\beta}H$); 51.1 (C^6). $^{31}P\{^1H\}$ NMR (CD_3OD): δ/ppm = 52.0. ^1H NMR (D_2O): δ/ppm = 8.41, 8.40, 8.33 (d, 3H, $^3J_{HH}$ = 2.9 Hz, $C^{\gamma}H$); 8.06 (d-br, 1H, $^3J_{HH}$ = 5.7 Hz, C^1H); 7.87 (td, 1H, $^3J_{HH}$ = 7.7 Hz, $^4J_{HH}$ = 1.4 Hz, C^3H); 7.49 (t, 3H, $^3J_{HH}$ = 7.4 Hz, $C^{10}H$); 7.43 (d, 1H, $^3J_{HH}$ = 7.9 Hz, C^4H); 7.34, 6.95, 6.95 (d, 3H, $^3J_{HH}$ = 2.3 Hz, $C^{\alpha}H$); 7.30 (t, 6H, $^3J_{HH}$ = 7.6 Hz, C^8H); 7.24 (t, 1H, $^3J_{HH}$ = 6.6 Hz, C^2H); 6.81 (t-br, 6H, C^9H); 6.41, 6.32, 6.31 (t, 3H, $^3J_{HH}$ = 2.6 Hz, $C^{\beta}H$); 4.27 (d, 1H, $^2J_{HH}$ = 16.7 Hz, C^6H); 3.33 (dd, 1H, $^2J_{HH}$ = 16.7 Hz, $^3J_{HH}$ = 6.0 Hz, C^6H); *NH_2 not observed.* $^{31}P\{^1H\}$ NMR (D_2O): δ/ppm = 52.7. Labeling refers to carbon atoms. Crystals suitable for X-ray diffraction were collected by slow diffusion of diethyl ether into a solution of **9** in dichloromethane/methanol mixture (approximately 1:1 v/v). Labeling refers to carbon atoms to carbon atoms as in the molecular drawing shown above.

[Ru(κ^3*N*-tpm)(κ^2*N*-1,10-phenanthroline)(PPh_3)][NO_3]$_2$ (**10**)

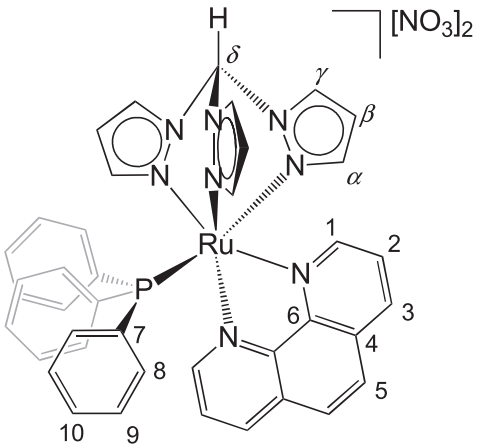

A mixture of **4** (100 mg, 0,11 mmol), phenanthroline (19.8 mg, 0.11 mmol) and $AgNO_3$ (37 mg, 0.22 mmol) in 5 mL of ethanol was heated at reflux for 6 h. The subsequent workup was performed following the procedure described for complex **8**. Orange solid, yield 79 mg (82 %). Anal. calcd. for $C_{40}H_{33}N_{10}O_6PRu$: C, 54.48; H, 3.77; N, 15.88. Found: C, 54.42; H, 3.52; N, 15.91. IR (solid state): $\tilde{u}/cm^{-1}$ = 3119 w, 3052 w, 2984 w, 2975 w, 2899 w, 1512 w, 1481 w, 1425 m, 1411 m, 1357 s ($\tilde{u}_{NO3}$), 1356 s ($\tilde{u}_{NO3}$), 1285 m, 1273 m, 1241 m, 1227 m, 1107 w, 1090 m, 1075 w, 1057 m, 853 m, 842 m, 829 w, 791 m, 776 m, 757 m, 744 m, 721 s, 692 s, 607 m, 525 s, 504 s, 459 m. ^{1}H NMR (CD_3OD): δ/ppm = 8.84 (dd, 2H, $^3J_{HH}$ = 5.3 Hz, $^4J_{HH}$ = 1.2 Hz, C^1H); 8.76 (m, 2H, $^3J_{HH}$ = 3.0 Hz, C^γH); 8.72 (dd, 2H, $^3J_{HH}$ = 8.2 Hz, $^4J_{HH}$ = 1.2 Hz, C^3H); 8.49 (d, 1H, $^3J_{HH}$ = 2.9 Hz, C^γH); 8.17 (s, 2H, C^5H); 7.92 (dd, 2H, $^3J_{HH}$ = 8.2 Hz, $^3J_{HH}$ = 5.2 Hz, C^2H); 7.48 (d, 2H, $^3J_{HH}$ = 2.3 Hz, C^αH); 7.37 (t, 3H, $^3J_{HH}$ = 7.4 Hz, C^{10}H); 7.12 (t, 6H, $^3J_{HH}$ = 7.8 Hz, C^8H); 6.65 (dd, 2H, $^3J_{HH}$ = 3.0 Hz, $^3J_{HH}$ = 2.3 Hz, C^βH); 6.29 (m, 8H, C^9H + C^αH + C^βH); *H_δ not observed.* ^{13}C NMR (CD_3OD): δ/ppm = 153.8 (C^1); 149.1, 143.1 (C^α); 148.3 (C^6); 137.3 (C^3); 136.1, 134.5 (C^γ); 132.6 (d, $^3J_{CP}$ = 9.6 Hz, C^8); 130.7 (C^4); 130.6 (C^7); 128.6 (d, $^2J_{CP}$ = 9.4 Hz, C^9); 127.9 (d, $^1J_{CP}$ = 43.4 Hz, C^7); 127.7 (C^5); 125.9 (C^2); 109.4 ($2C^\beta$); 108.8 (C^β); *C^δ not observed.* ^{31}P{^{1}H} NMR (CD_3OD): δ/ppm = 47.1. ^{1}H NMR (D_2O): δ/ppm = 8.75 (d, 2H, $^3J_{HH}$ = 5.3 Hz, C^1H); 8.61 (dd, 2H, $^3J_{HH}$ = 8.3 Hz, $^4J_{HH}$ = 1.2 Hz, C^3H); 8.56 (d, 2H, $^3J_{HH}$ = 3.0 Hz, C^γH); 8.29 (d, 1H, $^3J_{HH}$ = 2.8 Hz, C^γH); 8.09 (s, 2H, C^5H); 7.77 (dd, 2H, $^3J_{HH}$ = 8.2 Hz, $^3J_{HH}$ = 5.2 Hz, C^2H); 7.45 (d, 2H, $^3J_{HH}$ = 2.3 Hz, C^αH); 7.33 (t, 3H, $^3J_{HH}$ = 7.1 Hz, C^{10}H); 7.06 (t, 6H, $^3J_{HH}$ = 7.7 Hz, C^8H); 6.51 (t, 2H, $^3J_{HH}$ = 2.6 Hz, C^βH); 6.30 (t, 6H, $^3J_{HH}$ = 2.3 Hz, C^9H); 6.29 (m, 8H, C^8H + C^αH + C^βH); 6.16 (m, 1H, C^αH); 6.14 (m, 1H, C^βH); *C^δH not observed.* ^{31}P{^{1}H} NMR (D_2O): δ/ppm = 47.6. Labeling refers to carbon atoms as in the molecular drawing shown above.

General Procedure for Carbon Dioxide Catalytic Hydrogenation. In a typical experiment, the catalytic mixture containing solvent, catalyst, base and additive (if any) was prepared in a Schlenk tube under nitrogen and subsequently injected into a 40 mL magnetically stirred teflon-lined stainless steel autoclave built at CNR-ICCOM, kept under a nitrogen atmosphere. Then, the autoclave was pressurized with a H_2/CO_2 gas mixture at the desired pressure, placed into an oil bath preheated to the desired temperature and left stirring at 500 rpm for the set reaction time. After the run, the autoclave was cooled to < 10 °C using an ice bath, the pressure was gently released and the reaction mixture was transferred into a round bottom flask. The autoclave beaker was thoroughly rinsed with H_2O and the washings added to the rest of the mixture. The volume of the mixture was then gently reduced using a rotary evaporator at room temperature until a homogeneous mixture was obtained. DMF (300 μL) was added to the mixture as internal standard and the formate content was determined by integration of the corresponding ^{1}H NMR signal vs. DMF. D_2O (ca. 0.7 mL) was added as deuterated solvent. All tests were repeated at least twice to check for reproducibility (average error ca. 6 %).

CRediT authorship contribution statement

Sylwia Kostera: Writing – original draft, Methodology, Investigation, Data curation, Conceptualization. **Alberto Gobbo:** Methodology, Investigation, Data curation, Conceptualization. **Massimo Guelfi:** Investigation, Data curation. **Stefano Zacchini:** Writing – review & editing, Investigation, Data curation. **Gabriele Manca:** Writing – original draft, Methodology, Investigation, Conceptualization. **Fabio Marchetti:** Writing – review & editing, Writing – original draft, Supervision, Formal analysis, Conceptualization. **Luca Gonsalvi:** Writing – review & editing, Writing – original draft, Supervision, Methodology, Funding acquisition, Formal analysis, Conceptualization.

Declaration of competing interest

The authors declare that they have no known competing financial interests or personal relationships that could have appeared to influence the work reported in this paper.

Acknowledgments

This research was funded by the European Union – NextGeneration EU from the Italian Ministry of Environment and Energy Security POR H2 AdP MMES/ENEA with involvement of CNR and RSE, PNRR - Mission 2, Component 2, Investment 3.5 “Ricerca e sviluppo sull’idrogeno”, CUP: B93C22000630006 and under the National Recovery and Resilience Plan (NRRP), Mission 4, Component 2, Investment 1.1, Call for tender No. 104 published on 2.2.2022 by the Italian Ministry of University and Research (MUR), funded by the European Union – NextGenerationEU – Project PRIN 20225N5T5B “ALCOVAL” – CUP B53D23015120006 - Grant Assignment Decree No. 1064 adopted on 18/07/2023 by the Italian Ministry of University and Research (MUR). Mr. Carlo Bartoli (CNR-ICCOM) is gratefully thanked for building and servicing the steel autoclaves used in this study. We acknowledge the CINECA award under the ISCRA initiative, for the availability of high-performance computing resources and support.

Appendix A. Supplementary data

Supplementary data to this article can be found online at https://doi.org/10.1016/j.jcat.2025.116231.

Data availability

No data was used for the research described in the article.

References

[1] Climate NASA Carbon Dioxide latest measurements. https://climate.nasa.gov/vital-signs/carbon-dioxide/?intent=121 2025 (accessed 15 March 2025).

[2] a) F. Nocito, A. Dibenedetto, Atmospheric CO_2 mitigation technologies: carbon capture utilization and storage, Curr. Opin. Green Sustainable Chem. 21 (2020) 34–43, https://doi.org/10.1016/j.cogsc.2019.10.002;
b) A. Kar, G.K.S. Goeppert, Prakash, integrated CO_2 capture and conversion to formate and methanol: connecting two threads, Acc. Chem. Res. 52 (2019) 2892–2903, https://doi.org/10.1021/acs.accounts.9b00324;
c) P. Styring, E.A. Quadrelli, K. Armstrong (Eds.), Carbon Dioxide Utilization: Closing the Cycle, first ed., Elsevier B.V., 2015;
d) G. Centi, G. Iaquaniello, S. Perathoner, Can we afford to waste carbon dioxide? Carbon dioxide as a valuable source of carbon for the production of light olefins, ChemSusChem 4 (2011) 1265–1273, https://doi.org/10.1002/cssc.201100313;
e) G.A. Olah, G.K.S. Prakash, A. Goeppert, Anthropogenic chemical carbon cycle for a sustainable future, J. Am. Chem. Soc. 133 (2011) 12881–12898, https://doi.org/10.1021/ja202642y.

[3] a) X.-F. Wu, M. Beller (Eds.), Chemical Transformations of Carbon Dioxide, in Topics in Current Chemistry Collections, first ed., Springer International Publishing, 2018;
b) M. Scott, B. Blas Molinos, C. Westhues, G. Franciò, W. Leitner, Aqueous biphasic systems for the synthesis of formates by catalytic CO_2 hydrogenation: integrated reaction and catalyst separation for CO_2-scrubbing solutions, ChemSusChem 10 (2017) 1085–1093, https://doi.org/10.1002/cssc.201601814;

c) M. Aresta, A. Dibenedetto, A. Angelini, Catalysis for the valorization of exhaust carbon: from CO_2 to chemicals, materials, and fuels, technological use of CO_2, Chem. Rev. 114 (2014) 1709–1742, https://doi.org/10.1021/cr4002758;
d) M. Peters, B. Koehler, W. Kuckshinrichs, W. Leitner, P. Markewitz, T.E. Müller, Chemical technologies for exploiting and recycling carbon dioxide into the value chain, ChemSusChem 4 (2011) 1216–1240, https://doi.org/10.1002/cssc.201000447;
e) E.E. Benson, C.P. Kubiak, A.J. Sathrum, J.M. Smieja, Electrocatalytic and homogeneous approaches to conversion of CO_2 to liquid fuels, Chem. Soc. Rev. 38 (2009) 89–99, https://doi.org/10.1039/B804323J;
f) M. Aresta, A. Dibenedetto, Utilization of CO_2 as a chemical feedstock: opportunities and challenges, Dalton Trans. (2007) 2975–2992, https://doi.org/10.1039/B700658F.

[4] a) J. Klankermayer, S. Wesselbaum, K. Beydoun, W. Leitner, Selective catalytic synthesis using the combination of carbon dioxide and hydrogen: catalytic chess at the interface of energy and chemistry, Angew. Chem. Int. Ed. 55 (2016) 7296–7343, https://doi.org/10.1002/anie.201507458;
b) W.-H. Wang, Y. Himeda, J.T. Muckerman, G.F. Manbeck, E. Fujita, CO_2 hydrogenation to formate and methanol as an alternative to photo- and electrochemical CO_2 reduction, Chem. Rev. 115 (2015) 12936–12973, https://doi.org/10.1021/acs.chemrev.5b00197;
c) J. Klankermayer, W. Leitner, Love at second sight for CO_2 and H_2 in organic synthesis, Science 350 (2015) 629–630, https://doi.org/10.1126/science.aac7997.

[5] J. Hietala, A. Vuori, P. Johnsson, I. Pollari, W. Reutemann, H. Kieczka, Formic Acid. Ullmann's Encyclopedia of Industrial Chemistry, Wiley-VCH, Weinheim, Germany, 2000.

[6] a) P.G. Jessop, F. Joó, C.-C. Tai, Recent advances in the homogeneous hydrogenation of carbon dioxide, Coord. Chem. Rev. 248 (2004) 2425–2442, https://doi.org/10.1016/j.ccr.2004.05.019;
b) F. Joó, Aqueous Organometallic Catalysis, Kluwer Academic Publishers, Dordrecht, 2001;
c) W. Leitner, E. Dinjus, F. Gassner, CO_2 chemistry, in: B. Cornils, W.A. Herrmann (Eds.), Aqueous-Phase Organometallic Catalysis, Wiley-VCH, Weinheim, 1998, pp. 486–498;
d) P.G. Jessop, T. Ikariya, R. Noyori, Homogeneous hydrogenation of carbon dioxide, Chem. Rev. 95 (1995) 259–272, https://doi.org/10.1021/cr00034a001;
e) W. Leitner, Carbon dioxide as a raw material: the synthesis of formic acid and its derivatives from CO_2, Angew. Chem. Int. Ed. 34 (1995) 2207–2221, https://doi.org/10.1002/anie.199522071.

[7] a) S. Kushwaha, J. Parthiban, S.K. Singh, Recent developments in reversible CO_2 hydrogenation and formic acid dehydrogenation over molecular catalysts, ACS Omega 8 (2023) 38773–38793, https://doi.org/10.1021/acsomega.3c05286.b)W.-H. Wang, X. Feng, M. Bao, Homogeneously catalyzed CO_2 hydrogenation to formic acid/formate by using precious metal catalysts. Chapter 2, pp. 13–52 in: Y. Himeda (Ed.), CO_2 hydrogenation catalysis, 1st Edition, 2021, Wiley-VCH, Weinheim, Germany.

[8] a) F. Bertini, N. Gorgas, B. Stöger, M. Peruzzini, L.F. Veiros, K. Kirchner, L. Gonsalvi, Efficient and mild carbon dioxide hydrogenation to formate catalyzed by Fe(II) hydrido carbonyl complexes bearing 2,6-(diaminopyridyl)diphosphine pincer ligands, ACS Catal. 6 (2016) 2889–2893, https://doi.org/10.1021/acscatal.6b00416;
b) Y. Zhang, A.D. MacIntosh, J.L. Wong, E.A. Bielinski, P.G. Williard, B. Q. Mercado, N. Hazari, W.H. Bersnkoetter, Iron catalyzed CO_2 hydrogenation to formate enhanced by Lewis acid co-catalysts, Chem. Sci. 6 (2015) 4291–4299, https://doi.org/10.1039/C5SC01467K;
c) O. Rivada-Wheelagan, A. Dauth, G. Leitus, Y. Diskin-Posner, D. Milstein, Synthesis and reactivity of iron complexes with a new pyrazine-based pincer ligand, and application in catalytic low-pressure hydrogenation of carbon dioxide, Inorg. Chem. 54 (2015) 4526–4538, https://doi.org/10.1021/acs.inorgchem.5b00366;
d) H. Fong, J.C. Peters, Hydricity of an Fe–H species and catalytic CO_2 hydrogenation, Inorg. Chem. 54 (2015) 5124–5135, https://doi.org/10.1021/ic502508p;
e) C. Ziebart, C. Federsel, P. Anbarasan, R. Jackstell, W. Baumann, A. Spannenberg, M. Beller, Well-defined iron catalyst for improved hydrogenation of carbon dioxide and bicarbonate, J. Am. Chem. Soc. 134 (2012) 20701–20704, https://doi.org/10.1021/ja307924a;
f) R. Langer, Y. Diskin-Posner, G. Leitus, L.J.W. Shimon, Y. Ben-David, D. Milstein, Low-pressure hydrogenation of carbon dioxide catalyzed by an iron pincer complex exhibiting noble metal activity, Angew. Chem. Int. Ed. 50 (2011) 9948–9952, https://doi.org/10.1002/anie.201104542;
g) C. Federsel, A. Boddien, R. Jackstell, R. Jennerjahn, P.J. Dyson, R. Scopelliti, G. Laurenczy, M. Beller, A Well-defined iron catalyst for the reduction of bicarbonates and carbon dioxide to formates, alkyl formates, and formamides, Angew. Chem. Int. Ed. 49 (2010) 9777–9780, https://doi.org/10.1002/anie.201004263.

[9] a) M.V. Vollmer, J. Ye, J.C. Linehan, B.J. Graziano, A. Preston, E.S. Wiedner, C. C. Lu, Cobalt-group 13 complexes catalyze CO_2 hydrogenation via a Co(−I)/Co(I) redox cycle, ACS Catal. 10 (2020) 2459–2470, https://doi.org/10.1021/acscatal.9b03534;
b) J. Choi, Y. Lee, Catalytic hydrogenation of CO_2 at a structurally rigidified cobalt center, Inorg. Chem. Front. 7 (2020) 1845–1850, https://doi.org/10.1039/C9QI01431D;
c) S.A. Burgess, K. Grubel, A.M. Appel, E.S. Wiedner, J.C. Linehan, Hydrogenation of CO_2 at room temperature and low pressure with a cobalt tetraphosphine catalyst, Inorg. Chem. 56 (2017) 8580–8589, https://doi.org/10.1021/acs.inorgchem.7b01391;
d) A.Z. Spentzos, C.L. Barnes, W.H. Bernskoetter, Effective pincer cobalt precatalysts for lewis acid assisted CO_2 hydrogenation, Inorg. Chem. 55 (2016) 8225–8233, https://doi.org/10.1021/acs.inorgchem.6b01454;
e) M.S. Jeletic, M.L. Helm, E.B. Hulley, M.T. Mock, A.M. Appel, J.C. Linehan, A Cobalt hydride catalyst for the hydrogenation of CO_2: pathways for catalysis and deactivation, ACS Catal. 4 (2014) 3755–3762, https://doi.org/10.1021/cs5009927;
f) M.S. Jeletic, M.T. Mock, A.M. Appel, J.C. Linehan, A cobalt-based catalyst for the hydrogenation of CO_2 under ambient conditions, J. Am. Chem. Soc. 135 (2013) 11533–11536, https://doi.org/10.1021/ja406601v;
g) Y.M. Badiei, W.H. Wang, J.F. Hull, D.J. Szalda, J.T. Muckerman, Y. Himeda, E. Fujita, Cp*Co(III) catalysts with proton-responsive ligands for carbon dioxide hydrogenation in aqueous media, Inorg. Chem. 52 (2013) 12576–12586, https://doi.org/10.1021/ic401707u;
h) C. Federsel, C. Ziebart, R. Jackstell, W. Baumann, M. Beller, Catalytic hydrogenation of carbon dioxide and bicarbonates with a well-defined cobalt dihydrogen complex, Chem, Eur. J. 18 (2012) 72–75, https://doi.org/10.1002/chem.201101343.

[10] a) C.M. Hert, J.B. Curley, S.P. Kelley, N. Hazari, W.H. Bernskoetter, Comparative CO_2 hydrogenation catalysis with MACHO-type manganese complexes, Organometallics 41 (2022) 3332–3340, https://doi.org/10.1021/acs.organomet.2c00295;
b) D. Wei, R. Sang, P. Sponholz, H. Junge, M. Beller, Reversible hydrogenation of carbon dioxide to formic acid using a Mn-pincer complex in the presence of lysine, Nat. Energy 7 (2022) 438–447, https://doi.org/10.1038/s41560-022-01019-4;
c) S. Kostera, S. Weber, M. Peruzzini, L.F. Veiros, K. Kirchner, L. Gonsalvi, Carbon dioxide hydrogenation to formate catalyzed by a bench-stable, non-pincer-type Mn (I) alkylcarbonyl complex, Organometallics 40 (2021) 1213–1220, https://doi.org/10.1021/acs.organomet.0c00710;
d) A.K. Schlenker, E.G. Christensen, A.A. Zhanserkeev, G.R. McDonald, E.L. Yang, K.T. Lutz, R.P. Steele, R.T. Van der Linden, C.T. Saouma, Role of ligand-bound CO_2 in the hydrogenation of CO_2 to formate with a (PNP)Mn catalyst, ACS Catal. 11 (2021) 8358–8369, https://doi.org/10.1021/acscatal.1c01709;
e) A. Kumar, P. Daw, N.A. Espinosa-Jalapa, G. Leitus, L.J.W. Shimon, Y. Ben-David, D. Milstein, CO_2 activation by manganese pincer complexes through different modes of metal–ligand cooperation, Dalton Trans. 48 (2019) 14580–14584, https://doi.org/10.1039/C9DT03088C;
f) A. Dubey, L. Nencini, R.R. Fayzullin, C. Nervi, J.R. Khusnutdinova, Bio-inspired Mn(I) complexes for the hydrogenation of CO_2 to formate and formamide, ACS Catal. 7 (2017) 3864–3868, https://doi.org/10.1021/acscatal.7b00943;
g) F. Bertini, M. Glatz, N. Gorgas, B. Stöger, M. Peruzzini, L.F. Veiros, K. Kirchner, L. Gonsalvi, Carbon dioxide hydrogenation catalysed by well-defined Mn(I) PNP pincer hydride complexes, Chem. Sci. 8 (2017) 5024–5029, https://doi.org/10.1039/C7SC00209B.

[11] a) B.G. Schieweck, N.F. Westhues, J. Klankermayer, A highly active non-precious transition metal catalyst for the hydrogenation of carbon dioxide to formates, Chem. Sci. 10 (2019) 6519–6523, https://doi.org/10.1039/C8SC05230A;
b) S.A. Burgess, A.J. Kendall, D.R. Tyler, J.C. Linehan, A.M. Appel, Hydrogenation of CO_2 in Water Using a Bis(diphosphine) Ni–H complex, ACS Catal. 7 (2017) 3089–3096, https://doi.org/10.1021/acscatal.7b00350;
c) R.C. Cammarota, M.V. Vollmer, J. Xie, J. Ye, J.C. Linehan, S.A. Burgess, A. M. Appel, L. Gagliardi, C.C. Lu, A bimetallic nickel-gallium complex catalyzes CO_2 hydrogenation via the intermediacy of an anionic d10 nickel hydride, J. Am. Chem. Soc. 139 (2017) 14244–14250, https://doi.org/10.1021/jacs.7b07911;
d) S. Enthaler, A. Brueck, A. Kammer, H. Junge, E. Irran, S. Gülak, Exploring the reactivity of nickel pincer complexes in the decomposition of formic acid to CO_2/H_2 and the hydrogenation of $NaHCO_3$ to HCOONa, ChemCatChem 7 (2015) 65–69, https://doi.org/10.1002/cctc.201402716;
e) C.C. Tai, T. Chang, B. Roller, P.G. Jessop, High-pressure combinatorial screening of homogeneous catalysts: hydrogenation of carbon dioxide, Inorg. Chem. 42 (2003) 7340–7341, https://doi.org/10.1021/ic034881x;
f) Y. Inoue, H. Izumida, Y. Sasaki, H. Hashimoto, Catalytic fixation of carbon dioxide to formic acid by transition-metal complexes under mild conditions, Chem. Lett. (1976) 863–864, https://doi.org/10.1246/cl.1976.863.

[12] G.A. Filonenko, R. van Putten, E.N. Schulpen, E.J.M. Hensen, E.A. Pidko, Highly efficient reversible hydrogenation of carbon dioxide to formates using a ruthenium PNP-pincer catalyst, ChemCatChem 6 (2014) 1526–1530, https://doi.org/10.1002/cctc.201402119.

[13] C.A. Huff, M.S. Sanford, Catalytic CO_2 hydrogenation to formate by a ruthenium pincer complex, ACS Catal. 3 (2013) 2412–2416, https://doi.org/10.1021/cs400609u.

[14] P. Munshi, A.D. Main, J.C. Linehan, C.-C. Tai, P.G. Jessop, Hydrogenation of carbon dioxide catalyzed by ruthenium trimethylphosphine complexes: the accelerating effect of certain alcohols and amines, J. Am. Chem. Soc. 124 (2002) 7963–7971, https://doi.org/10.1021/ja0167856.

[15] R. Tanaka, M. Yamashita, K. Nozaki, Catalytic hydrogenation of carbon dioxide using Ir(III)−pincer complexes, J. Am. Chem. Soc. 131 (2009) 14168–14169, https://doi.org/10.1021/ja903574e.

[16] T.J. Schmeier, G.E. Dobereiner, R.H. Crabtree, N. Hazari, Secondary coordination sphere interactions facilitate the insertion step in an Iridium(III) CO_2 reduction catalyst, J. Am. Chem. Soc. 133 (2011) 9274–9277, https://doi.org/10.1021/ja2035514.

[17] Y. Himeda, Conversion of CO_2 into formate by homogeneously catalyzed hydrogenation in water: tuning catalytic activity and water solubility through the

acid–base equilibrium of the ligand, Eur. J. Inorg. Chem. (2007) 3927–3941, https://doi.org/10.1002/ejic.200700494.
[18] J.F. Hull, Y. Himeda, W.-H. Wang, B. Hashiguchi, R. Periana, D.J. Szalda, J. T. Muckerman, E. Fujita, Reversible hydrogen storage using CO_2 and a proton-switchable iridium catalyst in aqueous media under mild temperatures and pressures, Nat. Chem. 4 (2012) 383–388, https://doi.org/10.1038/nchem.1295.
[19] A. Azua, S. Sanz, E. Peris, Water-soluble Ir^{III} N-heterocyclic carbene based catalysts for the reduction of CO_2 to formate by transfer hydrogenation and the deuteration of aryl amines in water, Chem. Eur. J. 17 (2011) 3963–3967, https://doi.org/10.1002/chem.201002907.
[20] S. Takaoka, A. Eizawa, S. Kusumoto, K. Nakajima, Y. Nishibayashi, K. Nozaki, Hydrogenation of carbon dioxide with organic base by $PC^{II}P$-Ir catalysts, Organometallics 37 (2018) 3001–3009, https://doi.org/10.1021/acs.organomet.8b00377.
[21] C. Liu, J.-H. Xie, G.-L. Tian, W. Li, Q.-L. Zhou, Highly efficient hydrogenation of carbon dioxide to formate catalyzed by iridium(III) complexes of imine–diphosphine ligands, Chem. Sci. 6 (2015) 2928–2931, https://doi.org/10.1039/C5SC00248F.
[22] a) C. Pettinari, R. Pettinari, Metal derivatives of poly(pyrazolyl)alkanes I. Tris (pyrazolyl)alkanes and related systems, Coord. Chem. Rev. 249 (2005) 525–543, https://doi.org/10.1016/j.ccr.2004.05.010;
b) M.D. Ward, J.A. McCleverty, J.C. Jeffery, Coordination and supramolecular chemistry of multinucleating ligands containing two or more pyrazolyl-pyridine 'arms', Coord. Chem. Rev. 222 (2001) 251–272, https://doi.org/10.1016/S0010-8545(01)00301-0;
c) C. Slugovc, I. Padilla-Martinez, S. Sirol, E. Carmona, Rhodium- and iridium-trispyrazolylborate complexes: C-H activation and coordination chemistry, Coord. Chem. Rev. 213 (2001) 129–157, https://doi.org/10.1016/S0010-8545(00)00365-9;
d) N. Kitajima, W.B. Tolman, Coordination chemistry with sterically hindered hydrotris(pyrazolyl)borate ligands: organometallic and bioinorganic perspectives, Prog. Inorg. Chem. 43 (1995) 419–531, https://doi.org/10.1002/9780470166444.ch5;
e) S. Trofimenko, Recent advances in poly(pyrazolyl)borate (scorpionate) chemistry, Chem. Rev. 93 (1993) 943–980, https://doi.org/10.1021/cr00019a006;
f) K. Niedenzu, S. Trofimenko, Pyrazole derivatives of boron, Top. Curr. Chem. 131 (1986) 1–37, https://doi.org/10.1515/9783112620588-001;
g) S. Trofimenko, in: Scorpionates, The Coordination Chemistry of Polypyrazolylborate Ligands, Imperial College Press, 1999, https://doi.org/10.1021/ja9957940;
h) S. Trofimenko, Coordination chemistry of pyrazole-derived ligands, Chem. Rev 72 (1972) 497–509, https://doi.org/10.1021/cr60279a003;
i) S. Trofimenko, Polypyrazolylborates, a new class of ligands, Acc. Chem. Res. 4 (1971) 17–22, https://doi.org/10.1021/ar50037a003;
j) S. Trofimenko, Boron-pyrazole chemistry. II. Poly(1-pyrazolyl)-borates, J. Am. Chem. Soc. 89 (1967) 3170–3177, https://doi.org/10.1021/ja00989a017.
[23] a) H.R. Bigmore, S.C. Lawrence, P. Mountford, C.S. Tredget, Coordination, organometallic and related chemistry of tris(pyrazolyl)methane ligands, Dalton Trans. (2005) 635–651, https://doi.org/10.1039/B413121E;
b) D.L. Reger, Tris(Pyrazolyl)methane ligands: the neutral analogs of tris (pyrazolyl)borate ligands, Comments Inorg. Chem. 21 (1999) 1–28, https://doi.org/10.1080/02603599908020413.
[24] a) J.M. Muñoz-Molina, T.R. Belderrain, P.J. Perez, Group 11 tris(pyrazolyl) methane complexes: structural features and catalytic applications, Dalton Trans. 48 (2019) 10772–10781, https://doi.org/10.1039/C9DT01661A;
b) L.M.D.R.S. Martins, A.J.L. Pombeiro, Tris(pyrazol-1-yl)methane metal complexes for catalytic mild oxidative functionalizations of alkanes, alkenes and ketones, Coord. Chem. Rev. 265 (2014) 74–88, https://doi.org/10.1016/j.ccr.2014.01.013;
c) L.M.D.R.S. Martins, C-scorpionate complexes: ever young catalytic tools, Coord. Chem. Rev. 396 (2019) 89–102, https://doi.org/10.1016/j.ccr.2019.06.009;
d) A. Gobbo, X. Ma, G. Ciancaleoni, S. Zacchini, L. Biancalana, M. Guelfi, G. Pampaloni, S.P. Nolan, F. Marchetti, Ruthenium(II) tris-pyrazolylmethane complexes in transfer hydrogenation reactions, Eur. J. Inorg. Chem. 26 (2023) e202300078, https://doi.org/10.1002/ejic.202300078.
[25] C. Yin, Z. Xu, S.-H. Yang, S.M. Ng, K.Y. Wong, Z. Lin, C.P. Lau, Promoting effect of water in ruthenium-catalyzed hydrogenation of carbon dioxide to formic acid, Organometallics 20 (2001) 1216–1222, https://doi.org/10.1021/om000944x.
[26] S.M. Ng, C. Yin, C.H. Yeung, T.C. Chan, C.P. Lau, Ruthenium-catalyzed hydrogenation of carbon dioxide to formic acid in alcohols, Eur. J. Inorg. Chem. (2004) 1788–1793, https://doi.org/10.1002/ejic.200300847.
[27] A.P.C. Ribeiro, L.M.D.R.S. Martins, A.J.L. Pombeiro, Carbon dioxide-to-methanol single-pot conversion using a C-scorpionate iron(II) catalyst, Green Chem. 19 (2017) 4811–4815, https://doi.org/10.1039/C7GC01993A.
[28] a) J. Cervinka, A. Gobbo, L. Biancalana, L. Markova, V. Novohradsky, M. Guelfi, S. Zacchini, J. Kasparkova, V. Brabec, F. Marchetti, Ruthenium(II)–tris-pyrazolylmethane complexes inhibit cancer cell growth by disrupting mitochondrial calcium homeostasis, J. Med. Chem. 65 (2022) 10567–10587, https://doi.org/10.1021/acs.jmedchem.2c00722;
b) A. Gobbo, S.A.P. Pereira, L. Biancalana, S. Zacchini, M.L.M.F.S. Saraiva, P. J. Dyson, F. Marchetti, Anticancer ruthenium(II) tris(pyrazolyl)methane complexes with bioactive co-ligands, Dalton Trans. 51 (2022) 17050–17063, https://doi.org/10.1039/D2DT03009H;
c) A. Gobbo, F. Chen, S. Zacchini, S. Gou, F. Marchetti, Enhanced DNA damage and anti-proliferative activity of a novel ruthenium complex with a chlorambucil-decorated ligand, J. Inorg. Biochem. 260 (2024), https://doi.org/10.1016/j.jinorgbio.2024.112703.
[29] J.M. Walker, A. McEwan, R. Pycko, M.L. Tassotto, C. Gottardo, J. Th'ng, R. Wang, G.J. Spivak, [Tris(pyrazolyl)methane]ruthenium complexes capable of inhibiting cancer cell growth, Eur. J. Inorg. Chem. (2009) 4629–4633, https://doi.org/10.1002/ejic.200900766.
[30] L. Biancalana, G. Ciancaleoni, S. Zacchini, G. Pampaloni, F. Marchetti, Carbonyl-isocyanide mono-substitution in $[Fe_2Cp_2(CO)_4]$: a re-visitation, Inorg. Chim. Acta 517 (2020) 120181, https://doi.org/10.1016/j.ica.2020.120181.
[31] N.R. Palepu, A.V. Rao, W. Kaminsky, M.R. Kollipara. CSD Communication (Private Communication), (2019), CCDC 1456697 and CCDC 1456696 – identifiers HOTPOY and HOTPEO.
[32] L. Link, R. Niewa, Polynator: a tool to identify and quantitatively evaluate polyhedra and other shapes in crystal structures, J. Appl. Crystallogr. 56 (2023) 1855–1864, https://doi.org/10.1107/S1600576723008476.
[33] L.D. Field, B.A. Messerle, L. Soler, I.E. Buys, T.W. Hambley, Polypyrazolylmethane complexes of ruthenium, J. Chem. Soc. Dalton Trans. (2001) 1959–1965, https://doi.org/10.1039/B103939N.
[34] S. Kostera, G. Manca, L. Gonsalvi, Carbon dioxide hydrogenation to formate catalyzed by a neutral, coordinatively saturated tris-carbonyl Mn(I)-PNP pincer-type complex, Chem. Eur. J. 29 (2023) e202302642, https://doi.org/10.1002/chem.202302642.
[35] W.H. Bernskoetter, N. Hazari, Reversible hydrogenation of carbon dioxide to formic acid and methanol: Lewis acid enhancement of base metal catalysts, Acc. Chem. Res. 50 (2017) 1049–1058, https://doi.org/10.1021/acs.accounts.7b00039.
[36] L. Pavlovic, K.H. Hopmann, Understanding the influence of Lewis acids on CO_2 hydrogenation: the critical effect is on formate rotation, Organometallics 42 (2023) 3025–3035, https://doi.org/10.1021/acs.organomet.3c00342.
[37] a) N. Jourabchian, K. Jurkowski, E.B. Bauer, Ruthenium complexes of the general formula $[RuCl_2(PHOX)_2]$ as precatalysts in propargylic substitution reactions, Catal. Commun. 106 (2018) 92–95, https://doi.org/10.1016/j.catcom.2017.12.014;
b) S.L. Dabb, B.A. Messerle, M.K. Smith, A.C. Willis, Ru and Os complexes containing a P, N-donor heterotopic ligand: the effect of solvent on stereochemistry, Inorg. Chem. 47 (2008) 3034–3044, https://doi.org/10.1021/ic7019044;
c) M.D. Palacios, M.C. Puerta, P. Valerga, A. Lledos, E. Veilly, Coordinatively unsaturated semisandwich complexes of ruthenium with phosphinoamine ligands and related species: a complex containing (R, R)-1,2-Bis((diisopropylphosphino) amino)cyclohexane in a new coordination form κ^3P, P', N-η^2-P, N, Inorg. Chem. 46 (2007) 6958–6967, https://doi.org/10.1021/ic700674c;
d) R. Frech, W. Huang, Anion-solvent and anion-cation interactions in lithium and tetrabutylammonium trifluoromethanesulfonate solutions, J. Solution Chem. 23 (1994) 469–481, https://doi.org/10.1007/BF00972613.